GRAPHENE BASED FRACTAL STRUCTURE 5G MICROSTRIP PATCH ANTENNA DESIGN, PRODUCTION AND ANALYSIS

Prepared By

Beyza Nur DEMIRKOPARAN

M. SC. THESIS

DEPARTMENT OF ELECTRICAL-ELECTRONICS ENGINEERING

SIVAS SCIENCE AND TECHNOLOGY UNIVERSITY

INSTITUTE OF GRADUATE STUDIES

June 2025

STATEMENT OF ETHICS

In this thesis, which I have prepared in accordance with the Thesis Writing Guidelines of the Graduate School of Sivas University of Science and Technology.

- I declare that the data, information, and documents presented in the thesis have been obtained within the framework of academic and ethical principles,
- That all information, documents, evaluations, and results have been presented in accordance with scientific ethics and moral standards,
- That all the works I have benefited from during this thesis study have been properly cited and referenced,
- That no alterations have been made to the data used,
- And that the work presented in this thesis is original.

I hereby accept responsibility for any loss of rights that may arise against me should any of these statements be proven otherwise.

……..
Beyza Nur DEMIRKOPARAN
20/06/2025

GRAFEN TABANLI FRAKTAL YAPIDA 5G MİKROŞERİT YAMA ANTEN TASARIMI, ÜRETİMİ VE ANALİZİ

(YÜKSEK LİSANS TEZİ)

Beyza Nur DEMIRKOPARAN

SİVAS BİLİM VE TEKNOLOJİ ÜNİVERSİTESİ
LİSANSÜSTÜ EĞİTİM ENSTİTÜSÜ

Haziran 2025

ÖZET

Bu tez çalışması, geniş bant frekans aralığı uygulamaları için geliştirilen grafen kaplı fraktal mikroşerit yama antenin tasarımı, simülasyonu, üretimi ve deneysel analizini kapsamaktadır. Antenin 3–12 GHz frekans aralığındaki performansı incelenmiştir. Tasarım süreci CST Microwave Studio yazılımı ile gerçekleştirilmiş ve FR-4 ile Rogers RT-5880 olmak üzere iki farklı alt tabaka için tasarım yapılmıştır. İki farklı alt tabakanın seçilmesinin nedeni Rogers RT-5880 alt tabakasının yüksek frekanslarda FR-4 alt tabakasına göre daha iyi çalıştığını göstermektir. Alt tabakaların belirlenmesinde sonra tasarım çalışmalarına başlanmıştır. Tasarımda fraktal yapılar kullanılması amaçlanmıştır. Fraktal yapıları seçmemizdeki neden, bu yapıların deterministik davranışları ve ayırt edici geometrileridir. Ayrıca, birçok tasarım denemesiyle amacımız, istenilen frekans bantlarında verimli çalışabilecek bir anten geliştirmektir. Fraktal desenler, grafenin atom ölçekli altıgen yapısından esinlenilerek yazar tarafından özgün olarak tasarlanmıştır. Antenin kaplamasında kullanılması amaçlanan indirgenmiş grafen oksit (rGO) şu şekilde elde edilmiştir. Öncelikle grafit temin edilmiştir. Daha sonra temin edilen grafitten modifiye Hummers yöntemi ile Grafen oksit (GO) sentezlenmiştir. Sonunda indirgenmiş grafen okside (rGO) dönüştürülmüş ve farklı voltaj/süre koşullarında elektroforetik biriktirme (EPD) tekniğiyle anten yüzeylerine kaplanmıştır. Üretilen antenler, vektör ağ analizörü (VNA) kullanılarak karakterize edilmiş ve elde edilen sonuçlar simülasyon verileriyle karşılaştırılmıştır. FR-4 anteni simülasyonda 4.5 GHz'de −24 dB, ölçümde 5.5 GHz'de −23.28 dB değerine ulaşmıştır; rGO kaplandığında bu değer 9.15 GHz'de −27.63 dB olmuştur. Rogers RT-5880 için simülasyon sonuçları 5.5 GHz'de −27.9 dB, 10 GHz'de -10.77 dB olmuştur. Rogers RT-5880 için ölçüm sonuçları ise 4.8 GHz'de -22.99 dB iken, rGO kaplama sonrası 11.1 GHz'de −27.1 dB'ye ulaşmıştır. Elde edilen bulgular, Rogers RT-5880 alt tabakasının, rGO entegrasyonunun ve fraktal yapıların, anten performansını artırmada etkili olduğunu ve kablosuz haberleşme sistemleri için güçlü adaylar olduğunu göstermektedir.

Bilim Kodu : 93415
Anahtar Kelimeler : Mikroşerit Yama Anten, Fraktal Anten, Grafen, Grafen Kaplı Anten, 5G Haberleşme, Geniş Bantlı Anten, Modifiye Hummers Metodu, Elektroforetik Kaplama (EPD)
Sayfa Adedi : 68
Danışman : Prof. Dr. Hüsnü Deniz BAŞDEMİR

GRAPHENE BASED FRACTAL STRUCTURE 5G MICROSTRIP PATCH ANTENNA DESIGN, PRODUCTION AND ANALYSIS

(M.Sc. THESIS)

Beyza Nur DEMIRKOPARAN

SİVAS UNIVERSITY OF SCIENCE AND TECHNOLOGY

INSTITUTE OF GRADUATE STUDIES

June 2025

ABSTRACT

This thesis covers the design, simulation, fabrication, and experimental analysis of a graphene-coated fractal microstrip patch antenna developed for wideband frequency applications. The antenna's performance was investigated within the frequency range of 3–12 GHz. The design process was carried out using CST Microwave Studio software, and two different substrates—FR-4 and Rogers RT-5880—were used in the design. The reason for selecting two different substrates was to demonstrate that Rogers RT-5880 performs better than FR-4 at high frequencies. Following the selection of substrates, the design process commenced with the aim of incorporating fractal structures. These structures were chosen due to their deterministic behavior and distinctive geometry. Additionally, through multiple design iterations, our goal was to develop an antenna capable of operating efficiently across the desired frequency bands. The fractal patterns were originally designed by the author, inspired by the atomic-scale hexagonal structure of graphene.

The reduced graphene oxide (rGO), intended for coating the antenna, was obtained as follows: First, graphite was procured and then converted into graphene oxide (GO) using a modified Hummers method. Finally, the GO was reduced to rGO and deposited onto the antenna surfaces using the electrophoretic deposition (EPD) technique under varying voltage/time conditions. The fabricated antennas were characterized using a vector network analyzer (VNA), and the results were compared with simulation data. For the FR-4 substrate, simulation showed −24 dB at 4.5 GHz, while measurements indicated −23.28 dB at 5.5 GHz. After rGO coating, the result improved to −27.63 dB at 9.15 GHz. For the Rogers RT-5880 substrate, simulation results were −27.9 dB at 5.5 GHz and −10.77 dB at 10 GHz, while measurement results were −22.99 dB at 4.8 GHz and improved to −27.1 dB at 11.1 GHz after rGO coating. The findings demonstrate that the Rogers RT-5880 substrate, the integration of rGO, and the use of fractal structures significantly enhance antenna performance, making them strong candidates for wireless communication systems.

Science Code : 93415

Key Words : Microstrip Patch Antenna, Fractal Antenna, Graphene, 5G Communication, Wideband Antenna, Modified Hummers Method, Electrophoretic Deposition (EPD)

Page Number : 68

Supervisor : Prof. Dr. Husnu Deniz BASDEMIR

THANKS

I would like to express my sincere gratitude to my esteemed advisor, Prof. Dr. Husnu Deniz BASDEMIR, for his invaluable guidance, constructive feedback, and continuous support throughout every stage of this thesis.

I would like to thank Prof. Dr. Emre BICER, Vice Rector for contributing to my scientific development during the thesis process and for granting access to laboratory facilities. I am also sincerely grateful to Lecturer Dr. Ali ALTUNTEPE for his valuable technical support in the graphene synthesis, coating, and measurement stages.

This study was supported by the Scientific Research Projects (BAP) Coordination Unit of Sivas University of Science and Technology under Project Number: 2023-GENL-Hav-0013. I sincerely thank the BAP office for their financial and academic support, which made this work possible.

I would also like to thank my family, whose unwavering emotional support, patience, and understanding have been a constant source of strength during this journey. I am additionally thankful to my friends and colleagues who have encouraged and motivated me throughout the thesis process.

Finally, I would like to express my heartfelt appreciation to all individuals and institutions who have contributed to this study in any capacity.

Beyza Nur DEMIRKOPARAN

TABLE OF CONTENTS

Page

LIST OF TABLES

Table **Page**

LIST OF FIGURES

SYMBOLS AND ABBREVIATIONS

The symbols and abbreviations used in this study are presented below with their explanations.

Symbols	Explanations
σ	Electrical conductivity
ε_r	Relative dielectric constant (of substrate)
ε_o	Permittivity of free space (8.854×10^{-12} F/m)
μ_0	Permeability of free space ($4\pi \times 10^{-7}$ H/m)
f_r	Resonant frequency
ω	Angular frequency (rad/s)
τ	Relaxation time (s)
μ_c	Chemical potential / Fermi energy (eV)
T	Temperature (Kelvin)
k_B	Boltzmann constant (1.38×10^{-23} J/K)
$\hbar$	Reduced Planck constant (1.054×10^{-34} J·s)
e	Elementary charge (1.602×10^{-19} C)
W	Patch width (mm)
L	Patch length (mm)
ΔL	Length extension due to fringing effects (mm)
dB	Decibel
λ	Wavelength (m)
Γ	Reflection coefficient
VSWR	Voltage Standing Wave Ratio
S_{11}	Voltage reflection coefficient at the input port (dB)

Abbreviations	Explanations
BAP	Scientific Research Projects Coordination Unit
CST	Computer Simulation Technology
EPD	Electrophoretic Deposition
FR-4	Flame Retardant Epoxy Laminate
GHz	Gigahertz (10^9 Hz)
GO	Graphene Oxide
H_2O_2	Hydrogen Peroxide
H_2SO_4	Sulfuric Acid
$KMnO_4$	Potassium Permanganate
MMIC	Monolithic Microwave Integrated Circuit
MPA	Microstrip Patch Antenna
MPAA	Microstrip Patch Antenna Array
PBG	Photonic Band Gap
PCB	Printed Circuit Board
PVA	Polyvinyl Alcohol
PVP	Polyvinylpyrrolidone
Raman	Raman Spectroscopy
rGO	Reduced Graphene Oxide
SEM	Scanning Electron Microscopy
SLS	Sodium Lauryl Sulphate
THz	Terahertz (10^{12} Hz)
WB	Wideband
VNA	Vector Network Analyzer

1. INTRODUCTION

Microwave systems are composed of passive and active components arranged to perform useful functions. The most common examples include radar systems and microwave communication systems. Since antennas are a fundamental component of both radar and communication systems, some of their basic properties will be addressed in this thesis (Gourav Misra, 2015). Microstrip patch antennas are commonly employed in diverse communication systems due to their compact electrical structure. They provide notable benefits in terms of ease of fabrication and design flexibility. Frequently cited in academic literature, these antennas apply to a broad spectrum of uses, ranging from consumer-level electronic devices to sophisticated military technologies (Constantine A. Balanis, 2016). Low-profile antennas have become essential in systems such as high-performance aircraft, satellites, missiles, and spacecraft, where constraints like size, weight, cost, aerodynamic requirements, performance, and ease of installation exist. Numerous civilian and governmental technologies also present similar design criteria, including mobile radio and wireless communication systems (Hossain et al., 2016). Microstrip patch antennas are ideally suited to fulfill these requirements. These low-profile antennas can seamlessly integrate with Monolithic Microwave Integrated Circuit (MMIC) designs. They are adaptable for use on planar and non-planar surfaces, can be manufactured cost-effectively using modern printed circuit techniques, and demonstrate robust mechanical strength when mounted on rigid structures. Furthermore, the choice of patch geometry and operating mode allows for considerable versatility in resonant frequency, polarization, radiation pattern, and impedance. In addition, incorporating elements such as pins or varactor diodes between the patch and the ground plane enables the design of reconfigurable systems whose electrical properties, namely resonance frequency, impedance, and polarization, can be dynamically adjusted (Warren L. Stutzman, 2012).

A narrow bandwidth may be desirable in specialized applications, particularly government security systems. However, several enhancement techniques have been proposed to improve antenna efficiency (up to approximately 90% when surface waves are excluded) and to expand the operational bandwidth (up to around 35%). One of the most common approaches involves increasing the substrate thickness (Mishra et al., 2024). Nevertheless, increasing the thickness of the substrate introduces surface waves, which are generally undesirable. These waves consume a portion of the power that would otherwise contribute to space wave

radiation, reducing overall radiation efficiency. As they propagate within the substrate, they scatter at discontinuities such as the edges of the dielectric or ground plane, causing degradation in both the radiation pattern and polarization characteristics of the antenna (Dobir Hossain et al., 2016; Pang & Wu, 2002; Qamar et al., n.d.).Using resonant cavity structures has proven effective in suppressing such surface waves while preserving a wide bandwidth (Younssi et al., n.d.). Techniques such as stacking microstrip elements have also enhanced bandwidth performance (Jung et al., 2024; Targonski et al., 1998). Furthermore, microstrip antennas may exhibit high electromagnetic signatures at off-resonant frequencies, may become physically large at VHF and UHF frequencies, and in large array configurations, there is often a trade-off between bandwidth and scanning capability (Balanis, 2024; Kazama, n.d.).

Despite numerous advancements in microstrip antenna design, challenges such as limited bandwidth, surface wave interference, and material limitations remain critical, particularly for 5G applications that demand compact size, wide bandwidth, and reconfigurability (Nagy, 2023).

Carbon atoms are organized in graphene, an allotrope of 3-D crystalline graphite, in a 2-D monolayer of hexagonal lattice that resembles a honeycomb. Due to its exceptional mechanical and electrical qualities, which have prompted the creation of numerous innovative systems and devices, it has garnered substantial attention over the past 10 years from various research communities in engineering and physics (Bonaccorso et al., 2010). Writing with a pencil creates graphene stacks on paper because the pencil's lead includes graphite, which comprises many graphene layers. Recent advances in optical microscopy technology have made it possible to examine atomically thin and experimentally 2-D materials such as graphene (Niu et al., 2020). Although graphene has been extensively explored in THz and optical domains, experimental validation of its influence on GHz-band microstrip antennas remains scarce, especially in practical, fabricated structures. Graphene was preferred in this study due to its high electromagnetic, mechanical, electrical, and thermal properties and the scarcity of such implementations in GHz antenna systems in existing literature. Another motivation is the tunability of graphene's conductivity via the Kubo formula, which enables dynamic antenna behavior control (Constantine A. Balanis, 2012).

Since the antenna frequency range is selected as 3–12 GHz, WB (wideband) antenna design is implemented. Among the frequency bands used in 5G, WB frequencies were chosen

because this range offers an optimal balance between coverage area and data transmission speeds (Rochman et al., 2025). WB) technology is one of the most promising solutions for future communication systems due to its high-speed data rate and excellent immunity to multipath interference. In this context, WB antenna design plays a unique role because it acts as a bandpass filter and reshapes the pulse spectrum, requiring careful optimization to avoid unwanted distortions. Some critical requirements in WB antenna design include ultra-wide bandwidth, directional or omnidirectional radiation patterns, consistent gain and group delay, high radiation efficiency, and low-profile structure (M. A. Peyrot-Solis et al., 2005).

In this study, the antenna pattern was selected by fractal structures based on the microstrip patch antenna. Fractal geometries have proven advantageous for miniaturization and multiband operation due to their recursive and space-filling nature (Karmakar, 2021). All necessary design parameters were calculated analytically and verified using CST Studio Suite. Furthermore, the synthesized reduced graphene oxide (rGO) from graphite was synthesized using the modified Hummers method, and its subsequent coating on FR-4 and Rogers RT-5880 boards via electrophoretic deposition was completed. Finally, the performance of both conventional and graphene-coated antennas was evaluated through simulations and verified via real-time measurements using a Vector Network Analyzer (VNA).

This study contributes to the existing body of knowledge by integrating deterministic fractal geometries with graphene-based substrates in GHz-band WB antennas. The combined use of advanced materials and geometries offers a novel pathway for compact, reconfigurable, and efficient antennas suitable for next-generation communication systems. The primary aim of this thesis is to design, simulate, fabricate, and evaluate the performance of a graphene-based fractal microstrip patch antenna operating in the 3–12 GHz WB frequency range and to compare simulation results with real-time experimental measurement.

2. LITERATURE REVIEW

The body of literature regarding antenna characteristics has experienced substantial evolution, particularly emphasizing fractal antenna structures, the incorporation of graphene within antennas, and the diverse application domains of microstrip antennas. This section seeks to explore several pertinent studies identified in existing literature.

In a study by Venkatrao and his team, a multiband antenna design utilizing the Minswoki fractal structure was proposed to meet the demands of the next generation of 5G technologies. This antenna is meticulously engineered to operate across seven distinct frequency bands, rendering it suitable for multiband 5G wireless communication systems. The incorporation of fractal geometry in the design facilitates a reduction in antenna size while preserving optimal bandwidth and radiation performance. The findings suggest that antenna designs based on Minswoki fractal structures are exceptionally effective for multiband applications, particularly in scenarios where spatial constraints necessitate compact structures (Venkatrao* et al., 2020). Moreover, the article authored by Paun and colleagues explores the design and advantages of a 5G antenna developed using Koch snowflake fractal geometry. The fractal structure is observed to enhance the antenna's electrical length, thereby enabling miniaturization and facilitating multiband operation. These characteristics ensure the antenna meets the wideband and multiband performance criteria for 5G applications. The study emphasizes the benefits of fractal geometries in antenna design, providing practical solutions for 5G technologies (Paun et al., 2025).

Microstrip patch antennas operating in the GHz and THz bands have been employed to address many device miniaturization challenges. However, bandwidth, gain, and directivity often exhibit reduced performance, primarily due to surface waves generated by the substrate thickness. When the substrate thickness is relatively thin, the antenna bandwidth decreases; conversely, the bandwidth increases when the substrate is significantly thick, but surface wave-induced losses also become more pronounced (Esin Chang et al., 1986).

Graphene stands out as an exceptional material due to its remarkable physicochemical properties. It features an extensive theoretical specific surface area (approximately 2630 m^2/g), exceptionally high intrinsic carrier mobility (~200,000 $cm^2/V \cdot s$), a high Young's modulus near 1.0 TPa, outstanding thermal conductivity (~5000 $W/m \cdot K$), notable optical transparency (~97.7%), and superior electrical conductivity. These attributes make it an

essential candidate for various advanced technological applications, particularly in transparent conductive films and electrodes (Allen et al., 2010).

Although the scientific interest in graphene has surged in the last two decades, experimental investigations have been ongoing for over 30 years. Its combination of mechanical robustness and structural flexibility allows for extensive chemical modifications and functional adaptations of its carbon framework. As illustrated in Figure 1, graphene exhibits a planar honeycomb lattice composed of two equivalent carbon atoms per unit cell. Each atom contributes a π-electron, producing a delocalized electronic structure that enhances electrical performance (Zhu et al., 2010).

The first isolation of graphene was achieved through a process called micromechanical exfoliation, whereby thin graphene layers were mechanically separated from graphite. This breakthrough technique enabled the fabrication of pristine graphene flakes and laid the foundation for experimental and theoretical progress in the field (W. Choi et al., 2010).

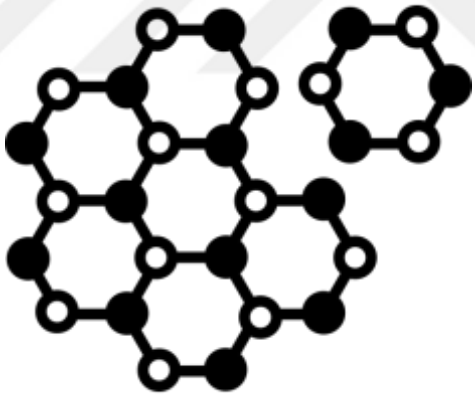

Figure 1. Crystal structure of graphene (W. Choi et al., 2010)

One of the most successful applications of graphene is in sensors, including gas and biosensors. The operating principle of graphene-based gas or bioelectronic sensors relies on the change in graphene's electrical conductivity (σ) due to the adsorption of molecules on its surface. The variation in conductivity can be attributed to changes in carrier concentration in graphene caused by the absorbed gas molecules acting as donors or acceptors. Additionally, some remarkable properties of graphene enhance its sensitivity, allowing for detection at the single-atom or single-molecule level. First, as a two-dimensional (2D)

material, the entire volume of graphene, meaning all carbon atoms, is exposed to the target analyte. Second, graphene exhibits low Johnson noise (electronic noise generated by thermal agitation, independent of any applied voltage), enabling even slight changes in carrier concentration to cause significant variations in electrical conductivity (W. Choi et al., 2010).

Moreover, graphene is a functional material with a zero bandgap, leading to broadband absorption properties and enabling relatively wide applications in photonics and nanoelectronics (see the energy band structure in Figure 2).

In addition to facilitating interband transitions between the valence and conduction bands, graphene also exhibits pronounced intraband absorption, making it highly suitable for terahertz (THz) wave applications such as detection, generation, and modulation (Falkovsky, 2008; Viti & Vitiello, 2021). When graphene absorbs THz photons, significant thermal gradients are generated. This is attributed to its low electron-specific heat, linear band structure, and rapid carrier thermalization dynamics, which together contribute to a pronounced nonlinear optical response under THz excitation (Brida et al., 2013; Hafez et al., 2018; Pop et al., 2012; Tielrooij et al., 2015).

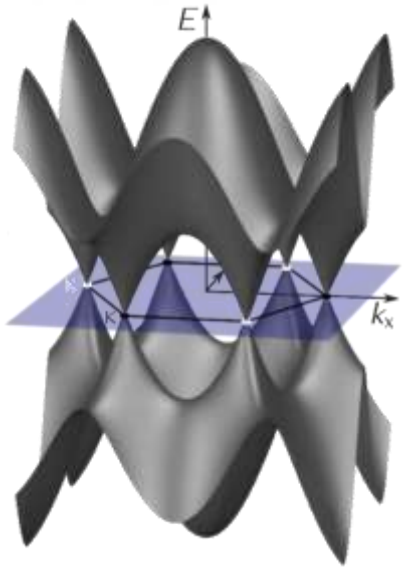

Figure 2. The schematic diagram of graphene's energy band structure. At the K point, the energy band structure of graphene is gapless and has a linear conical structure (Ponor, Electronic band structure of graphene, Wikimedia Commons, CC BY-SA 4.0).

The research conducted by Kumar and his team introduces a graphene-based microstrip patch antenna design that operates at a center frequency of 28.3 GHz, developed explicitly for 5G millimeter wave (mmWave) applications. This antenna is constructed on a substrate featuring a photonic crystal (PhC) structure, which is preferred over traditional dielectric materials to mitigate surface wave losses and enhance radiation efficiency, thereby improving overall antenna performance. Graphene is utilized as the patch component of the antenna, while copper serves as the ground plane. The three-dimensional configuration of the antenna has been meticulously modeled and analyzed using CST Microwave Studio software. Simulation results indicate that the antenna's S_{11} return loss is -33.69 dB, demonstrating excellent impedance matching and minimal reflection. Experimental measurements corroborate this, with an observed S_{11} value of -26.31 dB, which aligns closely with the simulation outcomes. The antenna's gain is reported to be approximately 5.5 dBi, and it operates with over 80% radiation efficiency. Incorporating the photonic crystal structure has significantly enhanced the antenna's bandwidth and directivity (radiation pattern) (Kumar et al., 2022).

In another antenna study, reconfigurable hybrid metal–graphene single/array rectangular microstrip patch antennas were simulated and optimized for 5G applications (Figure 3). The approach utilized in this study involves embedding graphene strips into a copper radiating patch to achieve a tunable antenna with reasonable performance (Marhoon & Qasem, 2020).

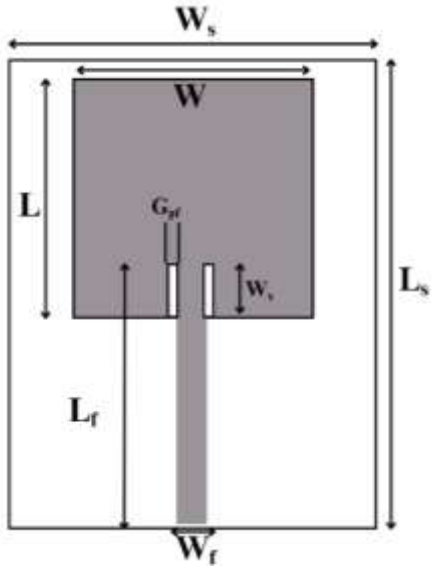

Figure 3. Single rectangular MPA and feedline (Marhoon & Qasem, 2020)

The designed antenna exhibits good gain and supports multiple frequencies in the 55.75 to 61.26 GHz range in a tunable single rectangular microstrip patch antenna (MPA). Similar results were obtained in the array configuration; however, the surface current distribution on the rectangular patch showed a slight shift toward a lower resonant frequency (fr).

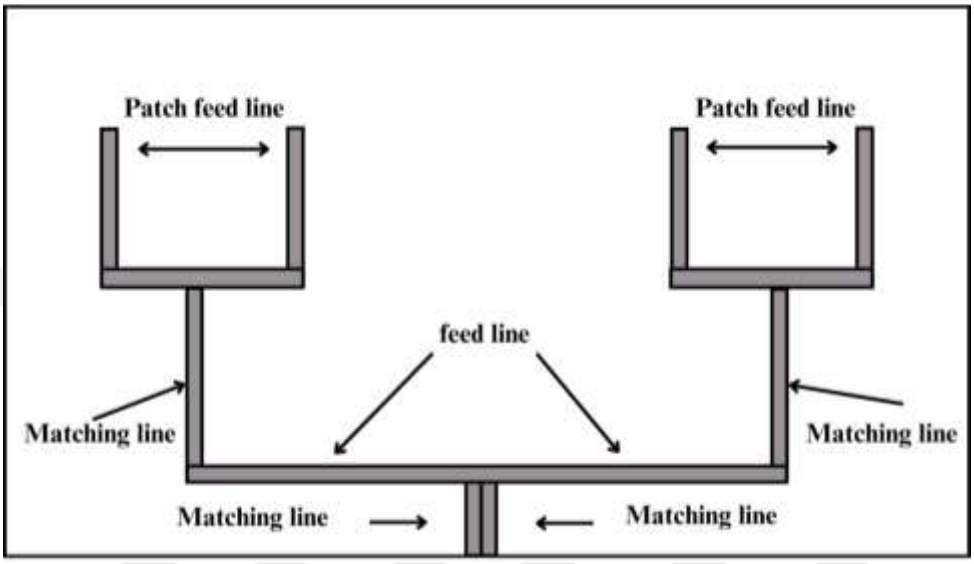

Figure 4. 4x1 Rectangular MPAA (Marhoon & Qasem, 2020)

The Microstrip Patch Array Antenna (MPAA) design differs from a single rectangular MPA in terms of current distribution. This variation is dependent on the voltage applied to the graphene strips. From this study, it can be concluded that increasing the voltage applied to the graphene strips reduces surface impedance, resulting in a shift of the resonance frequency toward higher values. Finally, the bandwidth of the MPA is extended. As the comparison results involving tunable single/array rectangular MPA designs mentioned above indicate, the antenna gain has been significantly improved (Figure 4) (Marhoon & Qasem, 2020).

Graphene-based microstrip antennas with Photonic Band Gap (PBG) substrates are considered strong candidates for addressing the challenges. In addition to forming TE and TM bandgaps, the proper arrangement of the periodic lattice enhances the antenna's bandwidth and efficiency. Considering these physical properties, this study presents significant results for a new graphene patch antenna operating in the GHz and THz bands, incorporating triangular air holes in the PBG substrate (Figure 5). As a result, the radiation characteristics of the antenna show notable improvement due to the use of a PBG substrate in the graphene-based patch antenna (Boutayeb & Denidni, 2007).

In the literature, studies on nano-patch antennas demonstrate successful results in reflection coefficient, radiation pattern, gain, and directivity by using a triangular periodic air-hole array with three different chemical potential values of graphene in three distinct configurations. Additionally, the resonant frequency shift of the antenna was confirmed with the formation of a second transmission band, showing that the antenna transitions from a single to a dual resonance state as the chemical potential gradually increased (de Sousa et al., 2023).

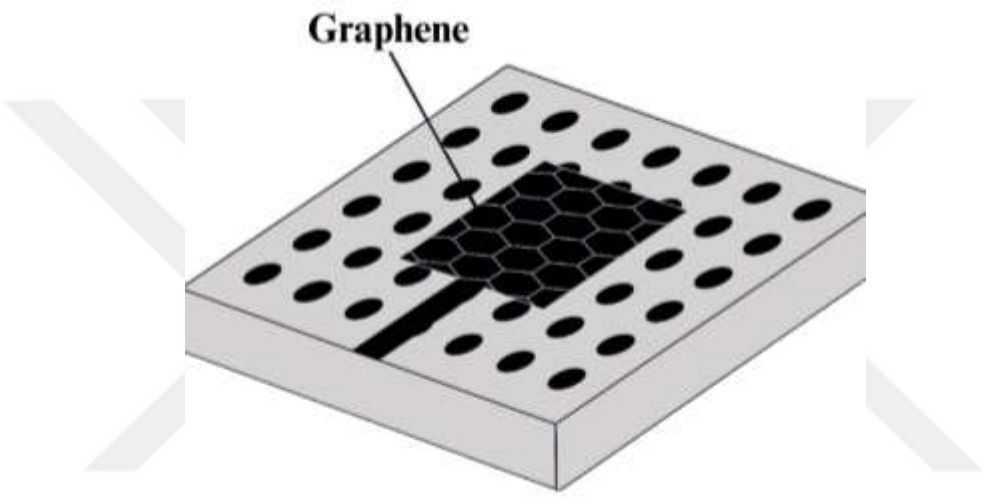

Figure 5. The graphene patch antenna is arranged with triangular lattice arrangements on the table(de Sousa et al., 2023).

Another notable study was conducted by Khani et al., in which a wave duplexer was designed using artificial graphene patterns to transmit incident waves into transmission and reflection channels. In this design, each multilayered structure consists of dielectric graphene patterns. Each component of the proposed device was modeled using passive circuit elements, and an equivalent impedance was calculated. The device was simulated using a full-wave numerical approach combined with an equivalent circuit model, with simulations carried out in CST software (Mohammad Khani et al., 2023). As previously discussed, graphene exhibits promising characteristics in GHz and THz frequency bands when integrated with Photonic Band Gap (PBG) substrates, yielding significant results in antenna performance. Therefore, one of the objectives of this study is to design, analyze, and evaluate the performance of a graphene-based microstrip patch antenna array employing fractal geometries. The antenna to be fabricated is designed to operate at a frequency range of 3-12

GHz, featuring a fractal structure and utilizing a microstrip transmission line feeding technique. Among the frequency bands used in 5G communications, the WB (Wide Band) range has been selected due to its balanced characteristics in terms of both coverage area and data transmission speed.

In the context of this thesis, copper surfaces were coated with graphene using the electrophoretic deposition (EPD) method. The EPD mechanism consists of two stages. In the first stage, charged particles move toward oppositely charged electrodes in the solution under a potential gradient generated by two electrodes. In the second stage, these particles accumulate on the electrode surfaces to form a deposit. Aqueous suspensions are preferred for EPD due to their environmental friendliness and cost-effectiveness. However, aqueous media become susceptible to electrolysis at higher voltage levels, resulting in gas formation at the electrodes, which can damage the deposits. Therefore, carefully selecting the applied voltage range is essential for achieving optimal coating quality (Jamil et al., 2021).

This thesis study selected the antenna pattern to conform to fractal structures based on the microstrip patch antenna layout. It has been demonstrated that by leveraging the recursive nature of fractals, several advantageous features can be achieved in antenna design and array performance (Karmakar, 2021). All relevant parameters were calculated theoretically and implemented using the CST Studio software. These parameters were further validated through simulation. Following the simulation phase, the reduction of graphene oxide to graphene and its deposition onto FR-4 plates was carried out and thoroughly explained.

3. MATERIALS AND METHODS

This thesis study aims to design microstrip patch antennas using graphene, determine their dimensions and operating frequency range through scientific computation methods, perform simulations using CST software, and fabricate prototype models based on the obtained results. Within this scope, the thesis will consist of the following stages.

3.1. Design and Analysis of Microstrip Patch Antennas Using CST Software

First and foremost, the conductivity of the graphene material to be used must be determined. Although the conductivity of graphene is inherently governed by its unique band structure, it also depends on several interrelated parameters, including chemical doping, Fermi energy (chemical potential), electron mobility, relaxation time, operating frequency, and ambient temperature. It is emphasized that these parameters are not mutually independent and can influence one another.

Under a semi-classical, local model and in the absence of an external magnetic field, graphene's conductivity can be modeled using the intraband contribution of the Kubo formula (Constantine A. Balanis, 2016) as follows:

$$\sigma = -j\frac{e^2 k_B T}{\pi\hbar^2(\omega - j\tau^{-1})}\ln\{2[1+\cos h\,(\frac{\mu_c}{k_B T})]\} \quad (1)$$

where:

- Elementary charge is e,
- Boltzmann constant is k_B,
- The absolute temperature is T,
- Reduced Planck constant is $\hbar$,
- Angular frequency is ω,
- Relaxation time is τ,
- Chemical potential (Fermi energy) is μ_c.

To ensure accurate modeling of the antenna, the dimensions of the microstrip patch must be calculated precisely. The design consists of a square patch positioned on a dielectric substrate with a relative permittivity (ε_r) placed above a perfect electric conductor (PEC) ground plane. The patch, assumed to be made of copper, is excited via a copper microstrip feed line.

As shown in Figure 6, the structure represents a typical microstrip patch antenna. When W/h > 1, surface wave excitation is reduced, and radiation efficiency increases. Narrow patches (i.e., W/h ≤ 1) confine more energy within the substrate as surface waves, which do not contribute to radiation and may cause interference or power loss. The effective dielectric constant, ε_{reff}, which accounts for the fringing fields, is calculated using the following empirical formula: microstrip patch antenna configuration. For microstrip antennas, the width-to-height ratio should satisfy W/h > 1(Constantine A. Balanis, 2016) (This will provide an explanation for the upcoming pages.).

$$\varepsilon_{reff} = \frac{\varepsilon_r + 1}{2} + \frac{\varepsilon_r - 1}{2}\left[1 + 12\frac{h}{w}\right]^{-1/2} \tag{2}$$

The width W of the patch is then determined using:

$$W = \frac{1}{2f_r\sqrt{\mu_0\varepsilon_0}}\sqrt{\frac{2}{\varepsilon_r + 1}} = \frac{v_0}{2fr}\sqrt{\frac{2}{\varepsilon_r + 1}} \tag{3}$$

Once *W* is calculated, the length extension ΔL, caused by fringing effects, is computed as:

$$\frac{\Delta L}{h} = 0.412\frac{\left(\varepsilon_{reff} + 0.3\right)\left(\frac{w}{h} + 0.264\right)}{\left(\varepsilon_{reff} - 0.258\right)\left(\frac{w}{h} + 0.8\right)} \tag{4}$$

Finally, the effective length L of the patch is calculated using:

$$L = \frac{1}{2f_r\sqrt{\varepsilon_{reff}}\sqrt{\mu_0\varepsilon_0}} - (2\Delta L) \tag{5}$$

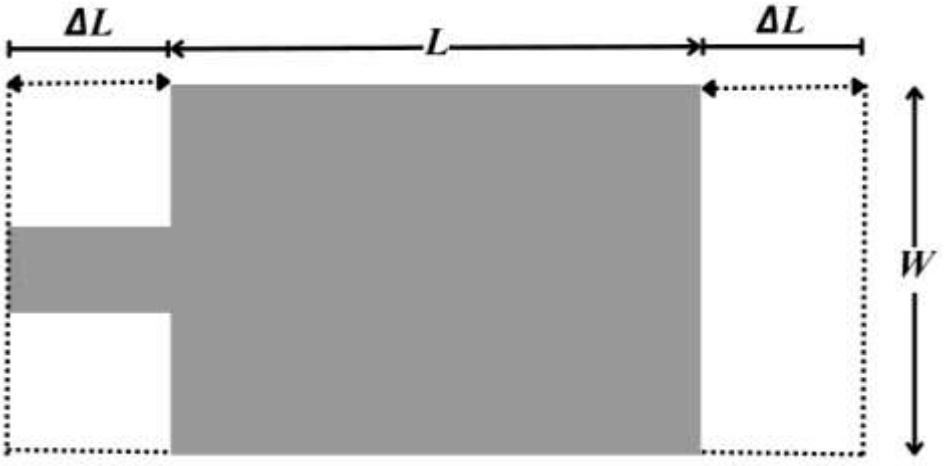

Figure 6. Physical lengths of microstrip patch (Constantine A. Balanis, 2016).

Calculations for both substrate materials were performed based on the relevant design equations and the specific electrical and physical properties of each substrate. Key parameters such as dielectric constant (εr), substrate thickness (h), and loss tangent (tan δ) were considered to accurately determine the patch dimensions, resonant frequency, effective dielectric constant, and impedance characteristics of the antenna structures. These calculations ensured that the designs for both the FR-4 and Rogers RT-5880 substrates were optimized for targeted frequency performance and efficient radiation behavior.

Table 1. Substrate size table

Substrate	**ε**	**h (mm)**	**Wp (mm) Calculated**	**Lp (mm) Calculated**	**ΔL (mm) Calculated**
FR-4	4.3	1.6	15.35	13.3	0.81
Rogers RT-5880	2.2	0.508	11.85	9.84	0.3

Using the derived equations, the fundamental geometry of the antenna was modeled in CST (Computer Simulation Technology) software (Figure 7). Dimensions are given for substrates in Table 1. Since the objective was to design a fractal structure, modifications were applied to align the geometry with fractal characteristics. These modifications were implemented through the integration of hexagonal (honeycomb) patterns. The design process has drawn inspiration from the atomic structure of graphene. The notches were introduced using the conventional 1/3 scaling ratio frequently employed in fractal antenna designs (Warren L. Stutzman, 2012). Similarly, the honeycomb configuration was constructed using comparable scaling principles. f_r denotes the desired resonance frequency, and c represents the speed of light. The antenna's bandwidth W_p depends on the substrate material's relative permittivity ε_r. To account for the influence of fringing fields extending beyond the radiating patch's physical boundaries, the effective dielectric constant ε_{reff} must be calculated and incorporated into the analysis (Süzgün & Cansiz, 2024).

Figure 7 illustrates the dimensions of the designed antenna. Figure 7 (a) shows the front view of the design, while Figure 7 (b) displays the back view. Fractal structures have optimized the dimensions of the front design. A feeding model commonly used in WB antennas has been employed for the antenna's rear feeding based on the width of the antenna. Three techniques were applied to design the WB antenna: first, the use of recessed structures;

second, the implementation of a partial ground plane; and third, the inclusion of a single slot in the patch to achieve good impedance matching. By selecting these parameters, the proposed antenna can be tuned to operate within the 3–12 GHz frequency range (S. H. Choi et al., 2004).

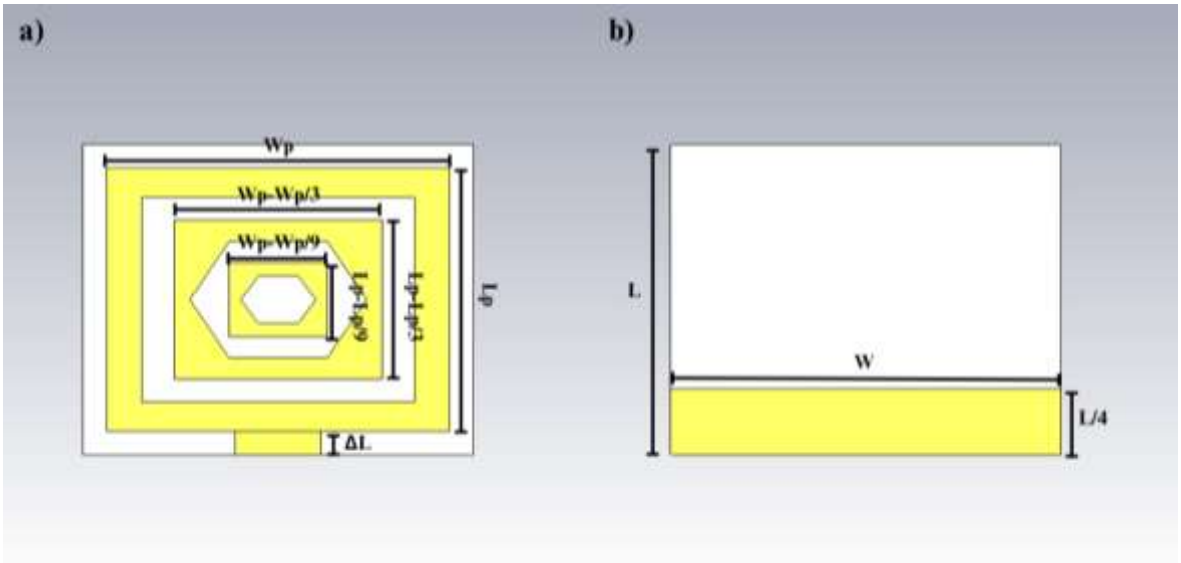

Figure 7. The CST-based design of the proposed antenna shows (a) the front view and (b) the back view of the structure.

3.2. Synthesis of Graphene

The reduced graphene oxide (rGO) utilized in this thesis study was synthesized from commercially supplied graphite powder through the Modified Hummers method, a widely recognized chemical oxidation process for producing graphene-based materials. This method enables the oxidation and exfoliation of graphite into graphene oxide (GO), which is then chemically reduced to obtain rGO with improved electrical conductivity.

Within the scope of this study, the synthesized rGO was subsequently utilized to enhance the electromagnetic properties of the microstrip patch antenna by electrophoretically depositing it onto the antenna surface. The electrophoretic deposition (EPD) technique was selected due to its simplicity, cost-effectiveness, uniform coating capability, and compatibility with complex geometries (BESRA & LIU, 2007). This approach allows the negatively charged rGO particles to migrate and deposit onto a positively charged electrode surface under the influence of an external electric field.

3.2.1. Preparation of Graphene Oxide

Graphene oxide (GO) was synthesized from graphite powder using a modified version of the Hummers method, a widely employed chemical oxidation technique for producing layered graphene derivatives. In this procedure, 1 g of graphite powder was initially combined with 0.5 g of sodium nitrate ($NaNO_3$) in a reaction vessel. Subsequently, 23 ml of concentrated sulfuric acid (H_2SO_4) was added dropwise under continuous magnetic stirring to ensure homogeneous mixing and to initiate the oxidation environment.

After allowing the mixture to stir for 1 hour, 3 g of potassium permanganate ($KMnO_4$) was slowly introduced while carefully maintaining the reaction temperature below 20 °C. This temperature control is essential to minimize the risk of thermal runaway and potential explosion, given the exothermic nature of the $KMnO_4$–H_2SO_4 interaction. Once the addition was complete, the mixture was stirred at an elevated temperature of 35 °C for 12 hours to allow sufficient oxidation of the graphite layers.

The highly viscous solution was then diluted with 500 ml of deionized water under vigorous stirring to terminate the oxidation process and begin exfoliation. To neutralize excess $KMnO_4$ and promote a complete reaction, 5 ml of 30% hydrogen peroxide (H_2O_2) was added. This step also causes a color change in the solution—typically from dark brown to yellow—indicating the formation of graphene oxide.

Finally, the mixture underwent a series of purification steps: it was washed sequentially with hydrochloric acid (HCl) and deionized water to remove metal ions and residual acid. The washed product was then filtered and oven-dried to yield fine, brownish graphene oxide powder. The morphology and consistency of the synthesized GO were visually confirmed, as shown in Figure 8 and Figure 9, which capture the key stages of the reaction and separation process (Liu et al., 2011).

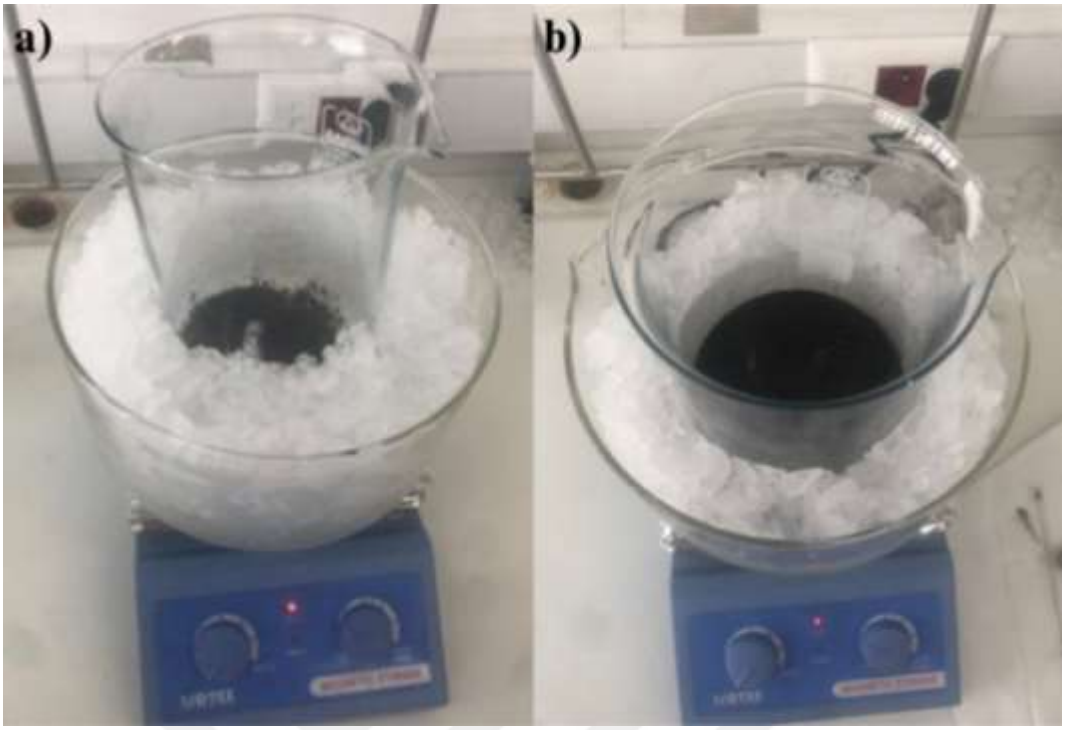

Figure 8. Mixing phase of graphite powder and sulfuric acid in the ice bath (a) the formation phase of graphite oxide left to stir in an ice bath (b)

Figure 9. Graphite oxide that settles to the bottom because of resting (a) The ultrasonic bathing phase of graphite oxide (b)

3.2.2. Dispersion of Graphene in Different Polar and Non-Polar Solvents

To investigate the dispersion behavior of graphene and to facilitate uniform distribution for further processing, graphene was dispersed in a variety of polar and non-polar solvents, namely water, chloroform, carbon tetrachloride, and hexane. The dispersion process was conducted using an ultrasonic bath, which aids in overcoming Van der Waals forces between graphene sheets, thereby improving exfoliation and dispersion stability (Dappe et al., 2006). Different concentrations of graphene were prepared by sonicating 50 mg of graphene in the respective solvents for a controlled duration.

A range of dispersing agents (surfactants and polymers) were employed to improve colloidal stability and to avoid agglomeration. These included:

- Anionic surfactants such as sodium dodecylbenzenesulfonate, sodium dodecylsulfonate, and sodium p-styrenesulfonate,
- Polyelectrolytes like poly(sodium p-styrenesulfonate) and sodium lignosulfonate,
- Classical surfactants, including sodium lauryl sulfate and cetyltrimethylammonium bromide,
- And water-soluble polymers such as polyvinylpyrrolidone (PVP) and polyvinyl alcohol (PVA).

Each dispersing agent was selected based on its molecular interaction potential with graphene surfaces and its compatibility with the chosen solvent system. The efficiency of dispersion was visually inspected and further characterized in subsequent steps, ensuring homogeneity before proceeding to electrophoretic deposition or coating processes.

3.2.3. Obtaining rGO by Reducing Graphene Oxide

Reduced graphene oxide (rGO) was synthesized through the chemical reduction of graphene oxide (GO), which was previously prepared via the modified Hummers method. In this procedure, 400 mg of dry GO powder was dispersed in 400 ml of distilled water. The suspension was subjected to vigorous magnetic stirring combined with ultrasonication for at least 1 hour, ensuring adequate exfoliation and homogeneity of the graphene oxide sheets within the aqueous medium.

The reduction process was initiated by adding hydrazine hydrate ($N_2H_4 \cdot H_2O$) as the chemical reducing agent, maintaining a 1:1 weight ratio of hydrazine hydrate to GO. The reduction was carried out at four different temperatures—15°C, 60°C, 80°C, and 95°C—to investigate the influence of thermal conditions on the quality and efficiency of the reduction reaction. Throughout the reaction, continuous stirring and intermittent ultrasonication were applied to facilitate uniform reduction and prevent restacking or aggregation of the sheets.

Upon completion of the reduction process, the resulting rGO precipitate was isolated by vacuum filtration and thoroughly washed with distilled water in four successive cycles to eliminate any residual reagents, byproducts, or unreacted hydrazine. The purified rGO was then subjected to thermal drying at 60°C for 24 hours in a laboratory oven to remove the remaining moisture and solvent residues. The final rGO product appeared as a fine black powder, indicating successful reduction (Figure 10) (Atiq Ur Rehman et al., 2021).

Figure 10. rGO formed from drying in the oven (Demirkoparan & Basdemir, 2024).

3.3. Electrophoretic Deposition (EPD) of Graphene Oxide onto the FR-4 Plates and Rogers RT-5880 Laminates

The Electrophoretic Deposition (EPD) process was conducted at ambient room temperature using a custom-fabricated electrochemical glass cell explicitly designed for coating planar substrates such as microstrip patch antennas. The deposition system employed a two-electrode configuration comprising a working electrode (WE) and a counter electrode (CE),

as illustrated in Figure 10. In this setup, the microstrip patch antenna itself served as the working electrode, which was connected to the anode terminal of a DC power supply. The counter electrode, connected to the cathode terminal, consisted of a straight iron wire acting as the auxiliary electrode. The spatial arrangement of the electrodes was carefully maintained, with a fixed inter-electrode distance of 10 cm, to ensure a uniform electric field distribution throughout the suspension medium. The electrolyte, which contained a homogeneous suspension of copper particles and reduced graphene oxide (rGO) in a suitable solvent, was continuously stirred magnetically at a rate of approximately 200 rpm during the deposition process. This stirring was essential to prevent particle sedimentation and to maintain consistent dispersion throughout the experiment.

Following the optimization of key EPD parameters, including voltage and deposition duration, the electrodes were connected to a regulated DC power supply, and deposition was initiated. Under the influence of the applied electric field, the negatively charged rGO and copper particles migrated toward the working electrode, where they were uniformly deposited onto the surface of the FR-4 substrate. The EPD experiments were performed using a range of voltage and time settings, as summarized in Table 2, to systematically study the influence of electrical parameters on coating morphology and thickness.

Table 2. EPD voltage and time values

No	Voltage (V)	Time (minute)
1	2.5	90
2	2.5	120
3	5	60
4	5	90
5	5	120
6	5	150
7	5	180
8	10	30
9	10	60

To achieve a comprehensive optimization of the Electrophoretic Deposition (EPD) process parameters, a series of controlled experiments were conducted in which reduced graphene oxide (rGO) was electrophoretically deposited onto the surface of the antenna structure under varying electrical and temporal conditions. Specifically, the applied deposition voltage was systematically adjusted across six levels: 10 V, 15 V, 20 V, 30 V, 40 V, and 50 V, while deposition durations were varied at 80, 120, 240, and 300 minutes, respectively.

This multi-level parameter matrix was designed to evaluate the influence of electric field strength and deposition time on coating quality, adhesion, film uniformity, and thickness. The experimental plan facilitated the identification of optimal process conditions that would yield consistent and homogenous rGO films with desirable electrical and structural properties. All experiments were carried out under identical environmental conditions, with continuous magnetic stirring of the electrolyte to maintain colloidal stability.

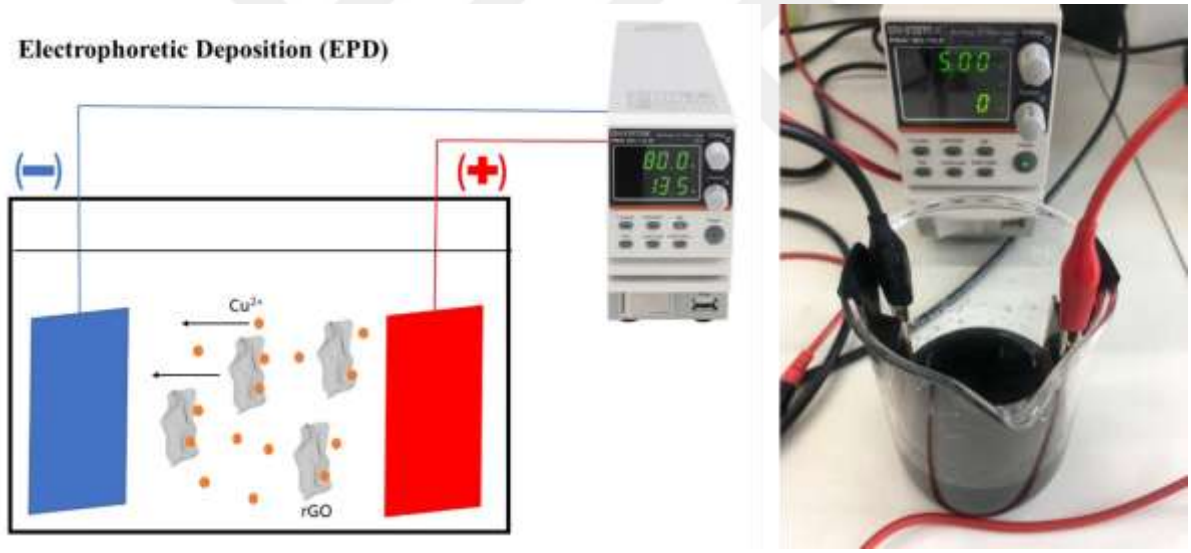

Figure 11. Electrophoretic deposition process

After completing the Electrophoretic Deposition (EPD) process, as illustrated in Figure 12, the coated samples were carefully removed from the electrochemical deposition cell and thoroughly rinsed with deionized water to eliminate any residual electrolytes or loosely bound particles from the surface. Following the rinsing step, the samples were gently air-dried at room temperature for several minutes to remove surface moisture and prevent thermal shock during subsequent heating.

Subsequently, the specimens were placed in a laboratory-grade convection oven and subjected to a thermal drying process at a constant temperature of 70 °C for 30 minutes (Figure 12). This controlled drying step was crucial to ensure the uniform evaporation of any remaining solvent and to enhance the adhesion and structural stability of the deposited reduced graphene oxide (rGO) layer. Maintaining a moderate temperature during drying also helped to avoid potential thermal degradation or delamination of the rGO coating from the FR-4 or Rogers RT-5880 substrates. After drying, the samples were allowed to cool gradually to room temperature under ambient conditions prior further characterization and analysis.

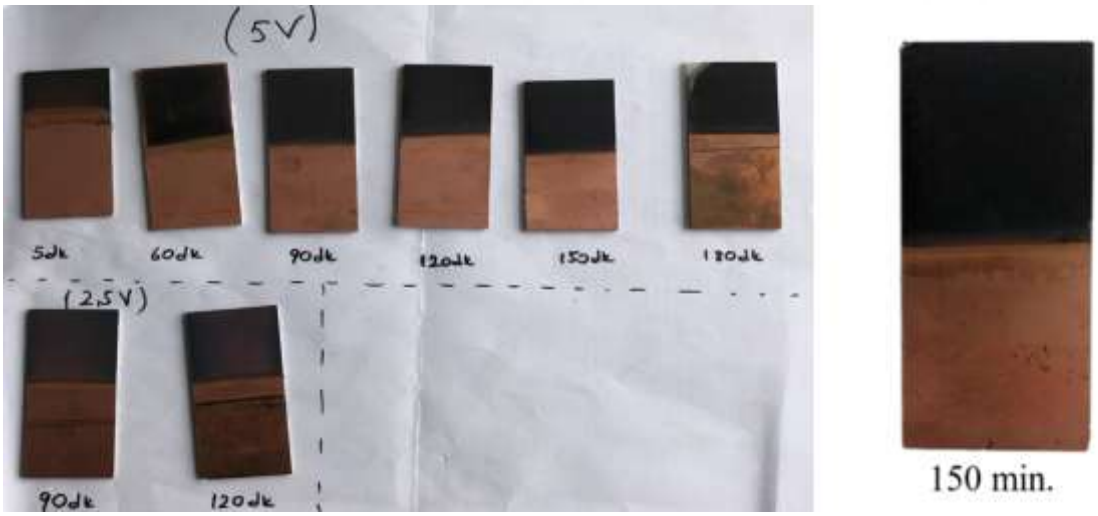

Figure 12. The plates were covered with the EPD process and the best-coated plate image at 5V for 150 minutes

After the EPD process, the samples were selected for Raman Spectrometry and Scanning Electron Microscopy (SEM) characterization. The thickness of the deposited FR-4 plates was measured using both an optical interferometer and SEM. Raman spectra indicated the occurrence of rGO deposition after electrophoretic deposition (Figure 13(a)) for samples 1 and 3, while the other samples showed an irregular surface of decomposed FR-4 plate. Deposited rGO was characterized via Raman spectroscopy. Carbon materials have three prominent peaks: the D, G, and 2D. These peaks help understand graphene film thickness, homogeneity, and quality by analyzing their position, sharpness, and intensity. The Raman spectrum of sample 1 and sample 2 rGO is shown in Figure 13 (a-b). Sample 1 has two prominent peaks: 1329 cm^{-1} for the D peak and 1596 cm^{-1} for the G peak, and sample 2 has prominent peaks: 1331 cm^{-1} for the D peak and 1592 cm^{-1} for the G peak, as expected. This

increase in D peak intensity is due to the GO reduction process, which leads to increased defect states in the structure.

Additionally, the I_D/I_G ratio provides insight into the hybridization (bond state) status of the rGO structure. In this context, the I_D/I_G ratio of sample 1 and 2 structure was determined to be 1.13 and 1.18, respectively. SEM images of samples 1 and 3 revealed a smooth rGO deposition between copper crystals (Figure 13).

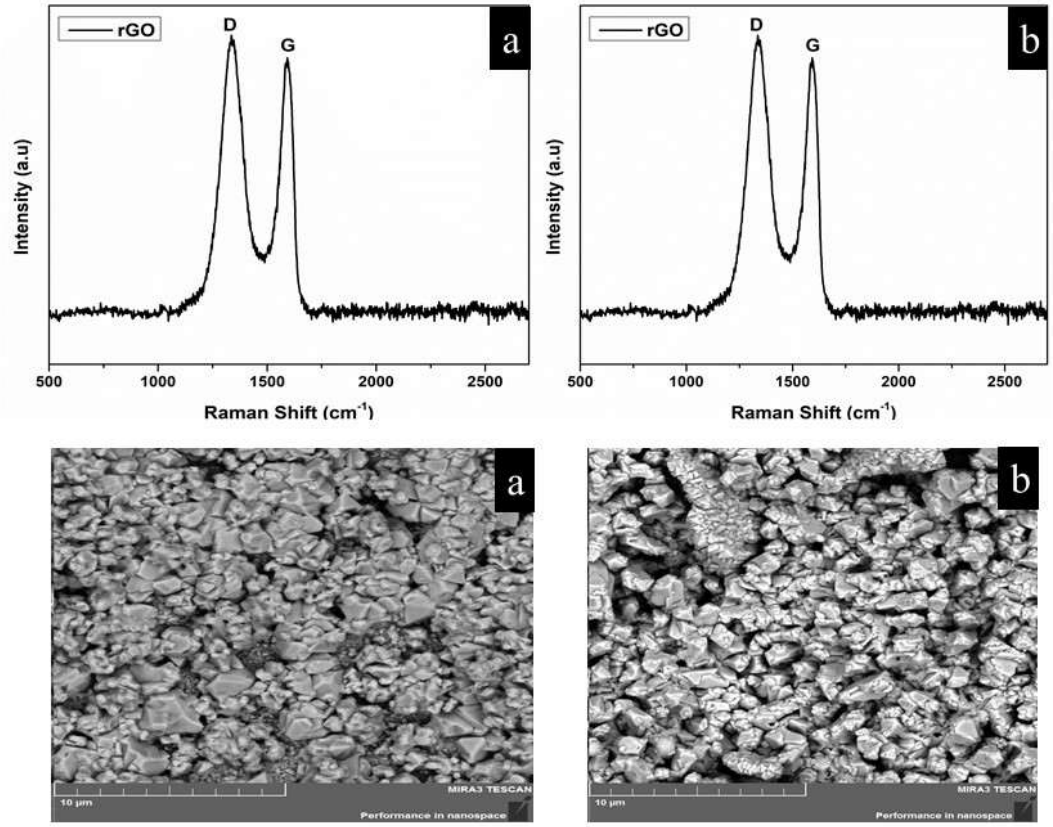

Figure 13. Raman spectra of (a) Sample 1 and (b) Sample 3. SEM pictures of (a) Sample 1 and (b) Sample 3

The thickness of the coatings obtained through Electrophoretic Deposition (EPD) was quantitatively evaluated using two distinct characterization techniques: optical interferometry and scanning electron microscopy (SEM) cross-sectional analysis. These complementary methods assessed the surface profile and the internal structural integrity of the deposited reduced graphene oxide (rGO) layers.

Based on optical interferometry measurements, Sample 1 exhibited a coating thickness of 1.5 to 2.0 µm, whereas Sample 3 demonstrated a relatively thicker layer, ranging from 3.0

to 4.0 µm. These measurements reflect the average vertical displacement across the coated surface under white-light interference conditions.

In contrast, the SEM cross-sectional imaging yielded differing results. For Sample 1, the measured coating thickness varied between 3.74 and 4.88 µm, while Sample 3 exhibited a thinner deposition, with values ranging from 1.20 to 1.45 µm (as illustrated in Figure 14). The discrepancy between the results obtained via the two methods can be primarily attributed to surface roughness and non-uniformity at different regions of the samples. While optical interferometry provides a broader surface average, SEM offers highly localized, high-resolution sectional data, which may capture thinner or thicker areas depending on the selected cross-sectional plane.

These differences highlight the importance of employing multiple complementary techniques for accurately characterizing nanostructured films deposited on non-ideal or heterogeneous surfaces.

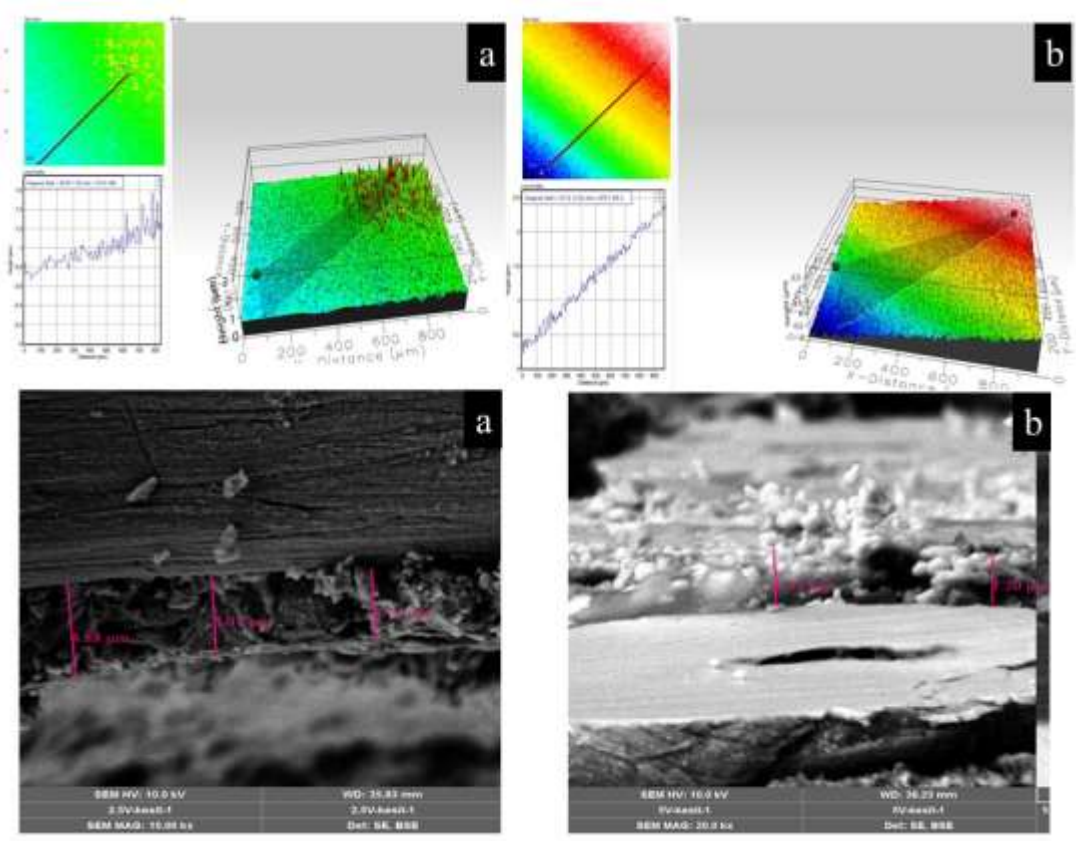

Figure 14. Optical interferometer analysis of (a) Sample 1 and (b) Sample 3. SEM cross-sectional thickness measurement results

3.4. Production of the Designed Antenna with PCB Etching Machine

In this thesis study, the fabrication of the proposed microstrip patch antenna prototypes were performed using a Printed Circuit Board (PCB) etching machine, as illustrated in Figure 15. This fabrication method provides a reliable and cost-effective approach for producing high-precision conductive patterns on copper-clad dielectric substrates, which are essential for realizing microstrip-based RF structures.

This technique allows for high dimensional accuracy, edge definition, and geometric consistency, all of which are critical for ensuring optimal electromagnetic behavior, especially at high-frequency ranges such as those used in WB and 5G applications. Accurate control over the patch geometry directly influences key antenna parameters including resonance frequency, impedance matching, and radiation efficiency (John Coonrod, 2023).

The PCB etching process also offers flexibility for fabricating antennas on various substrate types such as FR-4 and Rogers RT-5880, making it a versatile choice for prototyping and comparative performance evaluation across different dielectric materials.

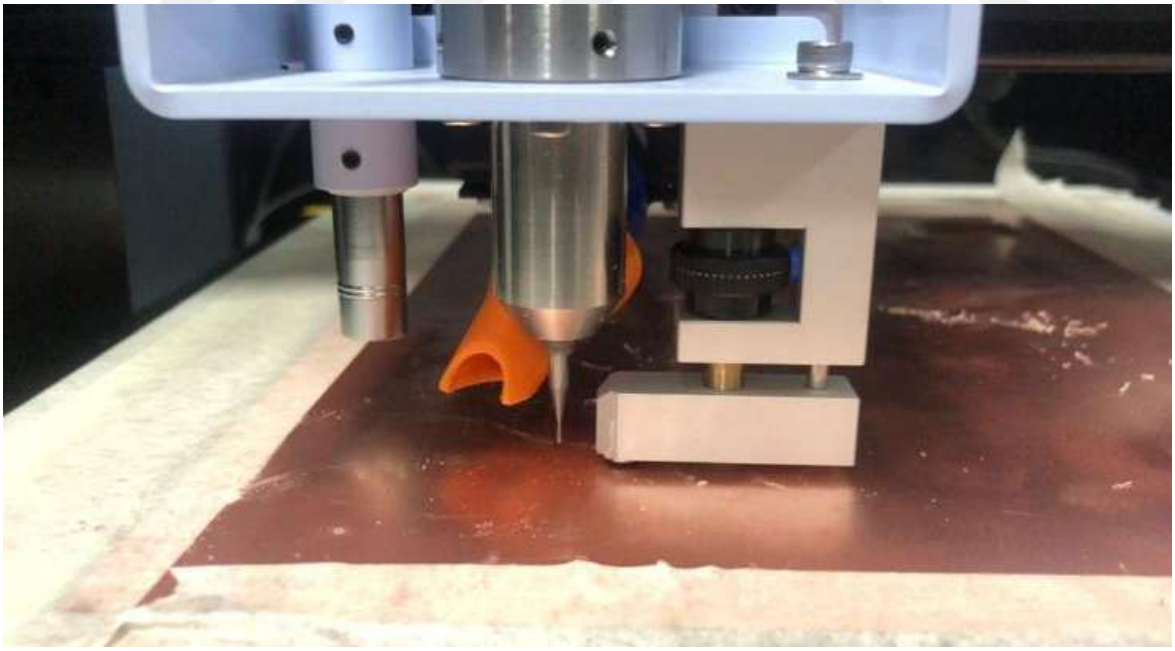

Figure 15. PCB etching process

Figure 16 presents the step-by-step development of the antenna prototypes fabricated through the etching process. In Figure 16 (a), the unprocessed copper plate is shown prior to any surface modification or patterning. This stage represents the raw conductive substrate,

which serves as the starting point for both standard and graphene-integrated antenna configurations.

Figure 16 (b) displays the etched copper pattern after the antenna design has been transferred onto the surface and the unwanted copper has been removed. Following the patterning process, the surface of this etched structure was subsequently coated with reduced graphene oxide (rGO) using the Electrophoretic Deposition (EPD) method, forming a hybrid conductive layer to improve electrical performance.

In the subsequent stages, advanced substrate materials were employed to evaluate performance under different dielectric conditions. Figure 16 (c) shows the mechanical scraping or shaping process applied to the Rogers RT-5880 laminate—an industry-standard low-loss substrate known for its superior high-frequency characteristics. The geometry of the antenna was precisely defined through mechanical or laser-based machining techniques, ensuring alignment with the simulation specifications. Figure 16 (d) illustrates the final fabrication stage involving the graphene-coated Rogers RT-5880 substrate. In this case, the same patterning and shaping methods were applied to the RT-5880 board after it had undergone EPD-based graphene deposition. This combination aimed to enhance the antenna's conductivity, reduce losses, and extend the usable bandwidth—making it highly suitable for wideband (WB) and 5G mid-band frequency applications.

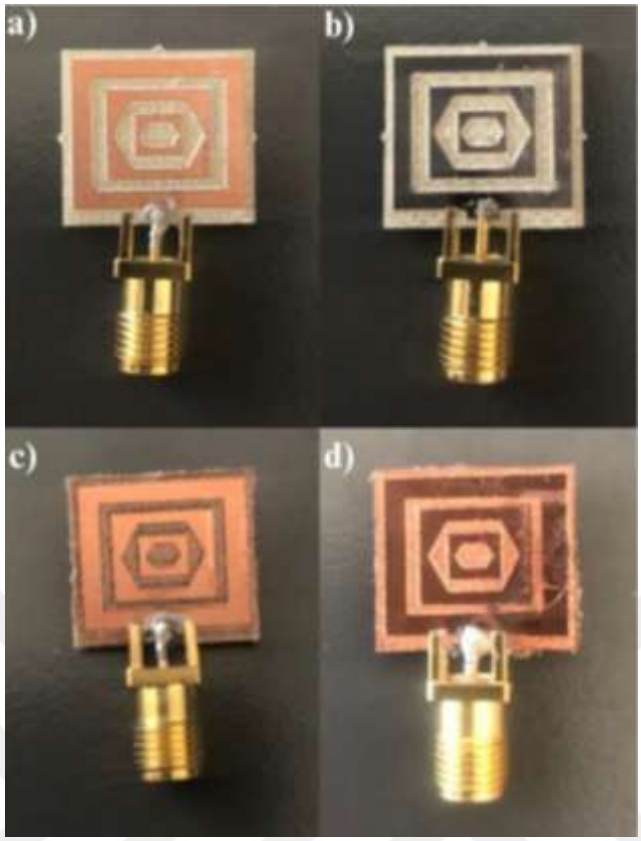

Figure 16. The fabricated prototype of the designed antenna (a) only a copper-coated FR-4 plate, (b) graphene-coated FR-4 plate, (c) only a copper-coated Rogers RT-5880, (d) graphene-coated Rogers RT-5880.

4. FINDINGS AND DISCUSSION

This section presents a comprehensive analysis that compares the simulation results with real-time experimental measurements to evaluate the antenna's performance across different substrate configurations. Emphasis is placed on identifying correlations and discrepancies between the CST-based simulations and the data acquired via Vector Network Analyzer (VNA) measurements. The comparison highlights key performance indicators such as return loss (S_{11}), resonant frequency shifts, and bandwidth variation, thereby offering critical insights into the effects of substrate material, graphene coating, and design geometry on the overall electromagnetic behavior of the antenna system. This analysis not only validates the accuracy of the simulation models but also underscores the importance of material characterization and fabrication precision in high-frequency antenna applications.

4.1. Simulation Results

A rectangular microstrip patch antenna geometry based on an FR-4 substrate was created in the initial design phase. The relative permittivity (ε_r) of the FR-4 substrate was taken as 4.3, and the loss tangent ($\tan \delta$) was assumed to be 0.025. The substrate thickness was set to 1.6 mm, and the copper patch thickness was defined as 0.035 mm. The antenna was designed to operate at a center frequency of 4.5 GHz. Parameters such as patch length, width, ground plane dimensions, and feed point were analytically calculated and finalized using CST's parametric optimization tools. In antenna design, the S_{11} parameter (also known as return loss) is expected to be less than -10 dB. This indicates that at least 90% of the input power is effectively radiated or transmitted, while less than 10% is reflected, ensuring efficient impedance matching and antenna performance (Balanis, 2024). It is observed that the designed antenna exhibits a return loss of -24 dB at 4.5 GHz and -11.8 dB at 10.5 GHz, indicating excellent impedance matching and minimal reflection at the target frequency (Figure 17).

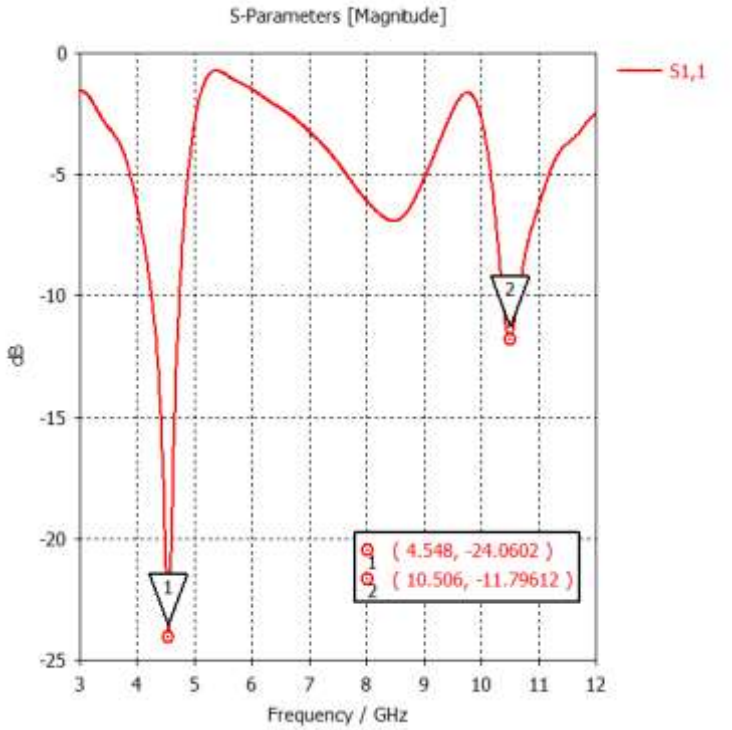

Figure 17. S_{11} parameter measured at 4.5 GHz using a copper-coated FR-4 board.

Voltage Standing Wave Ratio (VSWR) is a key parameter used in impedance matching between an antenna and the transmission line or source. It indicates how efficiently radio-frequency power is transmitted from the source to the load (i.e., the antenna) without being reflected.

Mathematically, VSWR is defined as:

$$VSWR = \frac{1+|\Gamma|}{1-|\Gamma|} \quad (6)$$

where Γ is the reflection coefficient, quantifying the signal's portion reflected due to impedance mismatch.

- VSWR = 1 means perfect matching – all the power is transmitted, and none is reflected.
- VSWR < 2 is generally considered acceptable in most antenna designs.
- VSWR > 2 indicates poor matching, leading to higher reflected power and reduced efficiency (Balanis, 2024).

In Figure 18, the VSWR values are at 4.5 GHz 1.13542 and at 10.5 GHz 1.695328, indicating an excellent impedance matching between the antenna and the transmission line, with minimal reflected power.

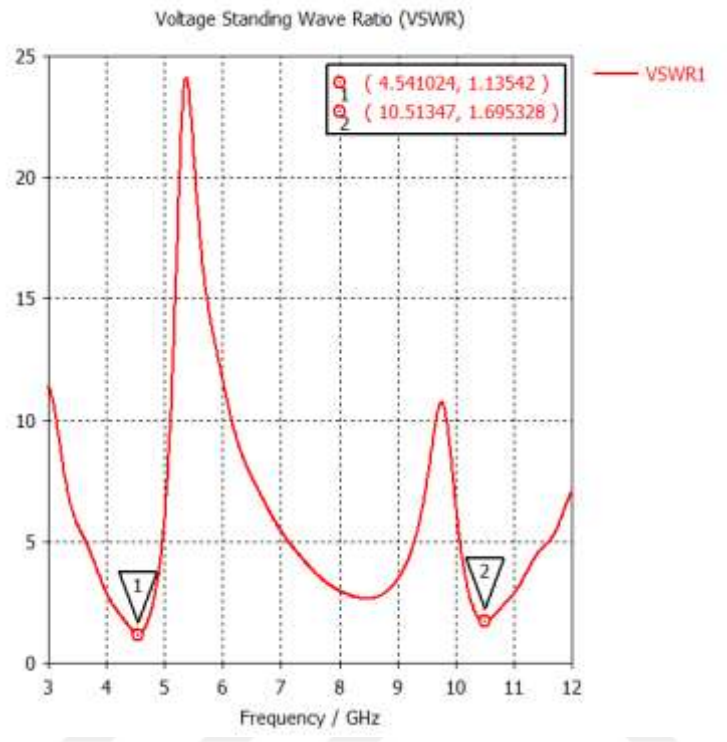

Figure 18. VSWR measurement for a copper-coated FR-4 plate at 4.5 GHz.

The polar gain plot represents the angular distribution of radiated electromagnetic power as a function of direction, measured at a constant distance within the antenna's far-field region. This plot provides critical insights into the directionality and radiation characteristics of the antenna. At the operating frequency of 4.5 GHz, the antenna demonstrates a distinct main lobe oriented along the $\varphi = 0°$ axis, with a peak gain amplitude of 2.98 dB, as depicted in Figure 19. This indicates that the antenna exhibits moderate directional behavior, efficiently radiating energy along the intended axis while minimizing side and back lobes, which is desirable in many communication applications where forward-directed transmission is prioritized.

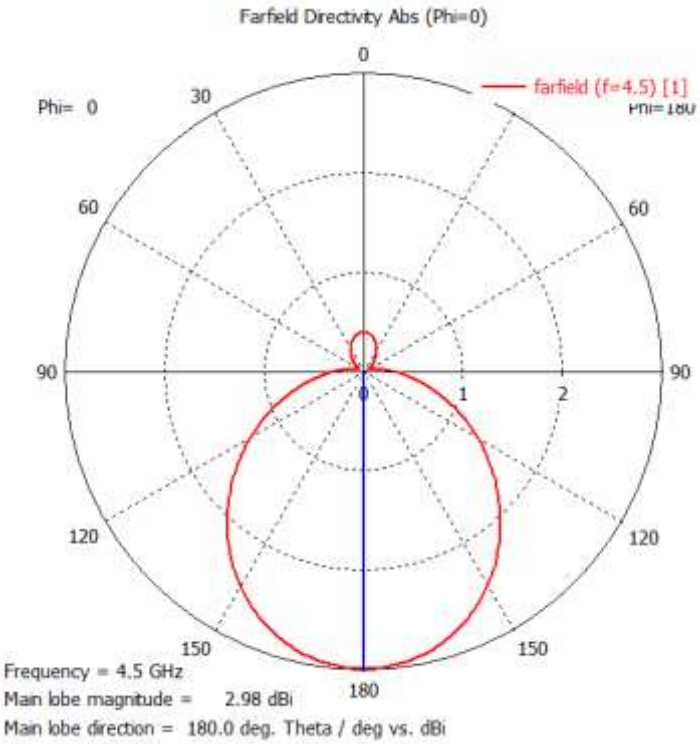

Figure 19. Polar radiation pattern for an FR-4 based antenna at 4.5 GHz.

Figure 20 illustrates the three-dimensional (3D) radiation pattern of the microstrip patch antenna fabricated on an FR-4 substrate, evaluated at the center frequency of 4.5 GHz. The 3D plot provides a detailed representation of the antenna's radiated power distribution in space, capturing the angular dependence of its radiation characteristics. The antenna exhibits a well-defined main lobe, confirming its directional radiation behavior in the far-field region. The directivity of the antenna at this frequency is measured to be 3.59 dB, indicating the extent to which the radiated energy is focused in the desired direction relative to an isotropic radiator. This value reflects a moderate enhancement in spatial selectivity, consistent with the antenna's intended design for targeted wireless communication applications.

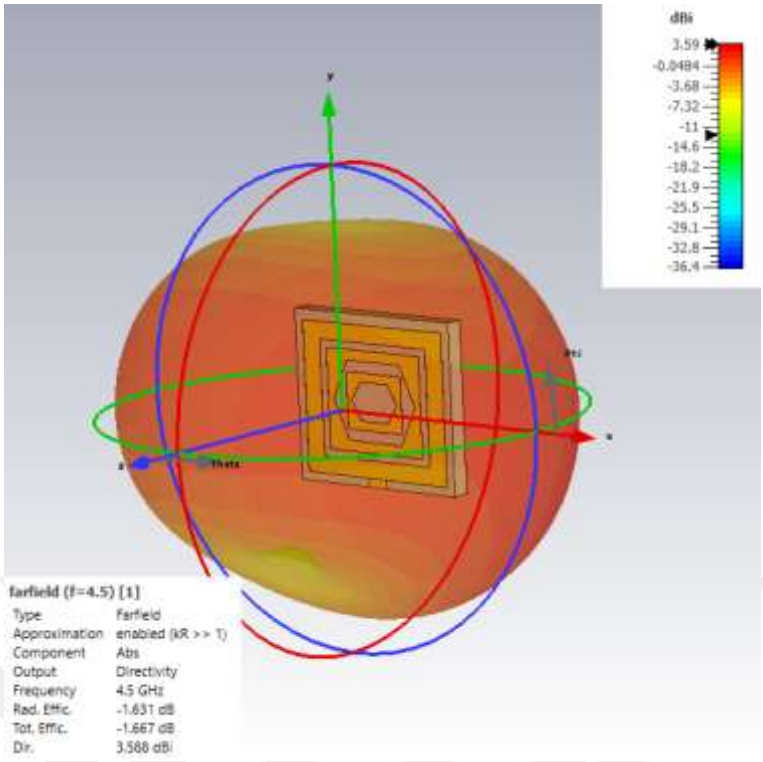

Figure 20. 3D radiation pattern of an FR-4 based antenna at 4.5 GHz.

The same simulation procedures applied to the FR-4 substrate were also performed for the Rogers RT-5880 substrate, which is known for its low dielectric loss and stable high-frequency performance. Accordingly, the patch width, substrate height, and feed line dimensions were recalculated to account for the material's different dielectric constant (ε_r) and loss tangent. Following these adjustments, the antenna design was simulated using CST Microwave Studio.

As shown in Figure 21, the simulated return loss at 5.9 GHz was observed to be approximately -22 dB. This value demonstrates excellent impedance matching, with minimal signal reflection at the feed point, indicating that a significant portion of the input power is effectively radiated. The result also confirms that the Rogers RT-5880 substrate contributes to improved high-frequency performance due to its superior dielectric properties compared to conventional materials such as FR-4.

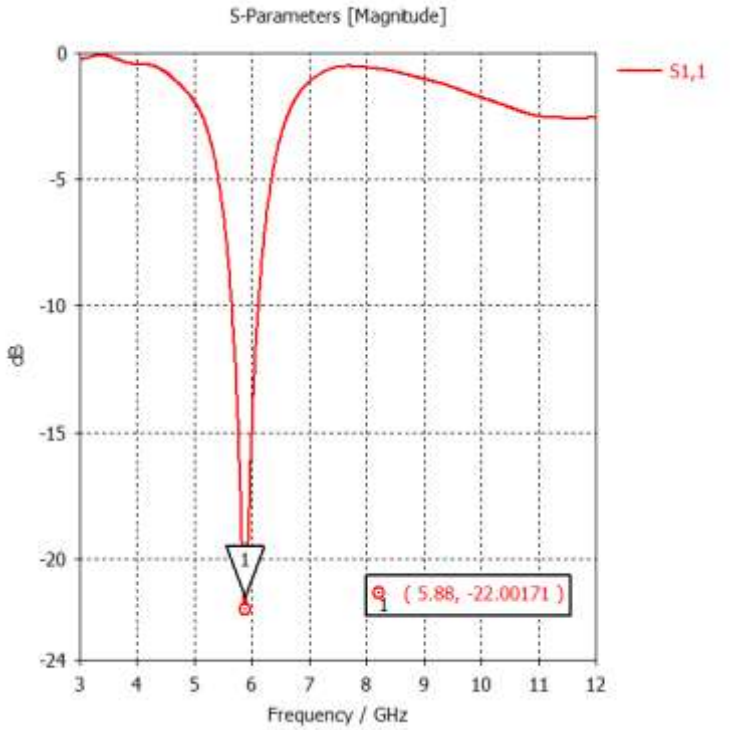

Figure 21. S_{11} parameter measured at 5.9 GHz using a copper-coated Rogers RT-5880 plate.

As illustrated in Figure 22, the Voltage Standing Wave Ratio (VSWR) for the antenna implemented on the Rogers RT-5880 substrate is measured 1.174513 at 5.9 GHz. This value indicates excellent impedance matching between the antenna and the connected transmission line, ensuring that most of the input power is delivered to the antenna with minimal reflected power. A VSWR value close to 1 signifies that the system experiences negligible mismatch losses, thereby enhancing overall antenna efficiency and transmission performance, particularly in high-frequency applications such as those targeted in this study.

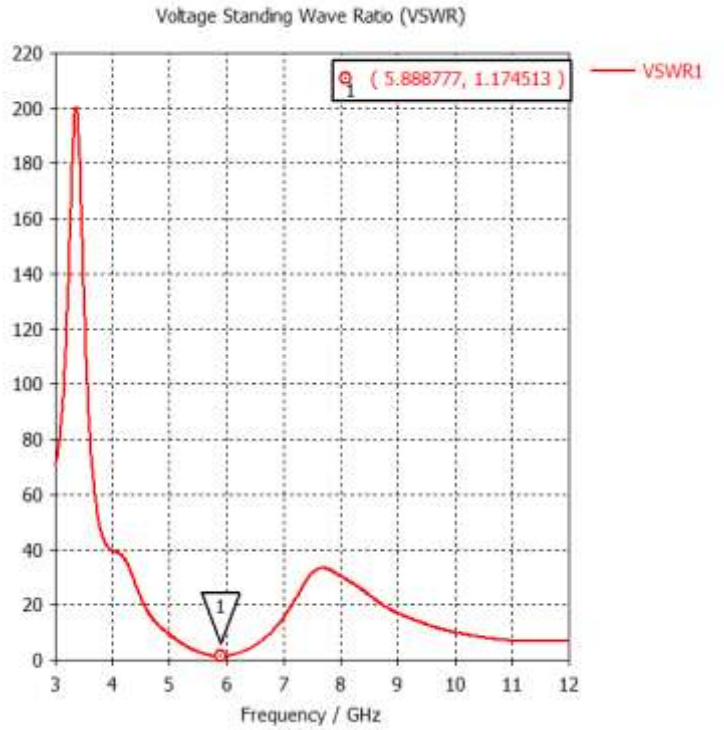

Figure 22. VSWR measurement for a copper-coated Rogers RT-5880 plate at 6.7 GHz.

The polar gain plot represents the angular distribution of the radiated electromagnetic field intensity at a constant distance within the far-field region of the antenna. This graphical depiction provides crucial insight into the antenna's directional radiation characteristics and is essential for evaluating angular coverage and field concentration performance. At the operating frequency of 5.5 GHz, the antenna fabricated on the Rogers RT-5880 substrate exhibits a prominent main lobe along the $\varphi = 0°$ axis, with a peak gain value of 3.95 dB, as shown in Figure 23. This indicates that the antenna maintains efficient directional radiation behavior, which is suitable for applications requiring focused energy transmission and reduced back or side lobes.

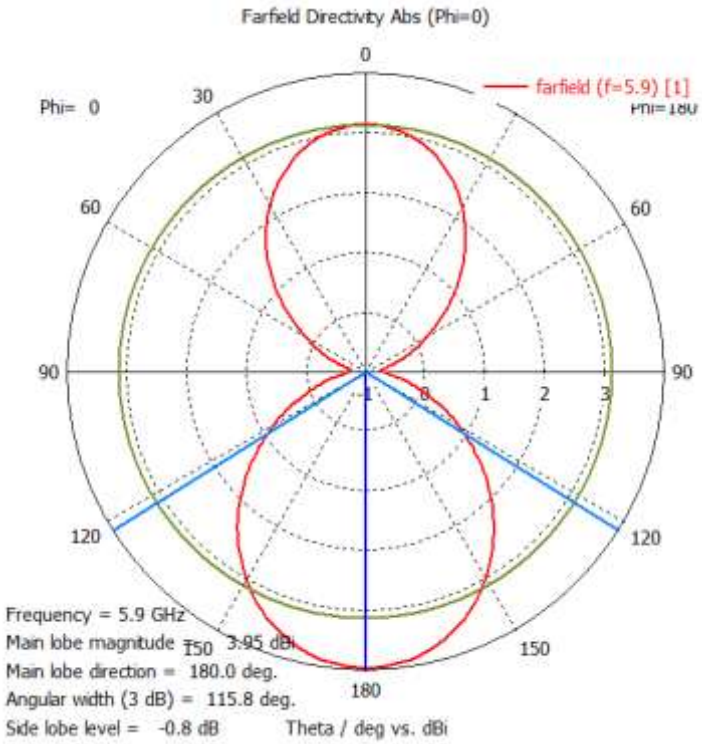

Figure 23. Polar radiation pattern for a Rogers RT-5880 based antenna at 5.9 GHz.

Figure 24 presents the three-dimensional (3D) radiation pattern of the microstrip patch antenna implemented on a Rogers RT-5880 substrate, evaluated at an operating frequency of 5.9 GHz. The radiation pattern offers a comprehensive spatial visualization of the antenna's far-field behavior, highlighting the directionality and distribution of radiated power. The measured directivity of the antenna at this frequency is 4.02 dB, indicating a moderate level of radiation concentration along the main lobe. This value confirms the antenna's capability to effectively focus energy on a desired direction, which is essential for reliable performance in high-frequency applications such as 5G mid-band communications.

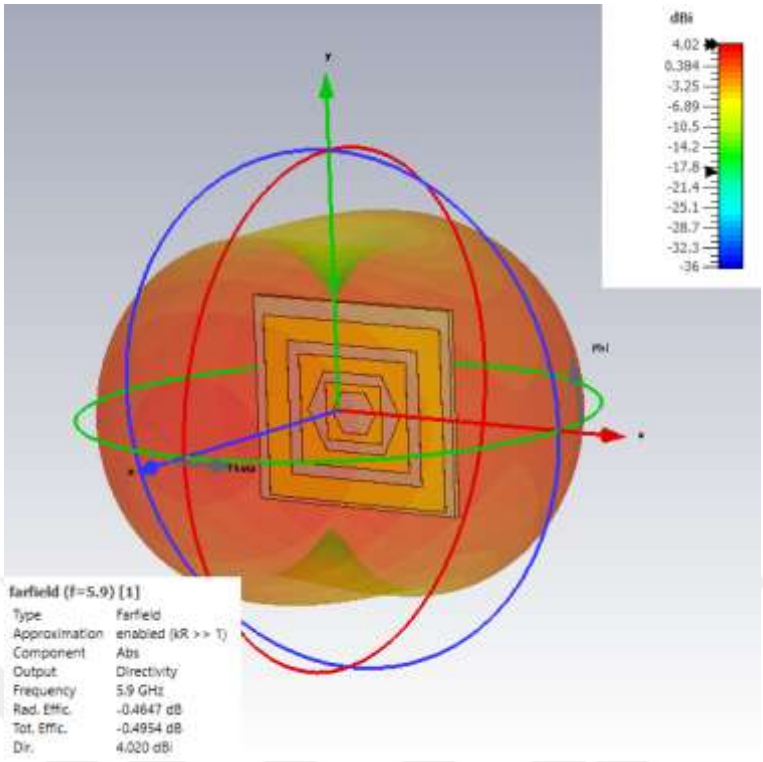

Figure 24. 3D radiation pattern of a Rogers RT-5880 based antenna at 5.9 GHz.

4.2. Real-Time Experimental Results

The subsequent phase of the thesis involved conducting real-time measurements utilizing a Vector Network Analyzer (VNA). A VNA is a device used to evaluate the frequency response of a single component or a network comprising multiple passive or active components. It assesses the power of a high-frequency signal as it enters and reflects from the device under test since power, unlike voltage or current, can be measured more precisely at elevated frequencies. At each frequency point, the VNA captures both the amplitude and phase of the signal. Using its internal processing unit, it calculates essential characteristics such as return loss and insertion loss and offers a variety of formats to display measurement results (Figure 25) (Zhang et al., 2015).

Figure 25. VNA measurement process.

The initial measurement derived from real-time assessments pertains to the FR-4 substrate. In this context, the S_{11} parameters were evaluated using a Vector Network Analyzer (VNA). The optimal S_{11} return loss for FR-4 substrates was recorded at 5.7 GHz, achieving a value of -23.28 dB. Notably, the observed value closely aligns with the simulation outcomes; however, a slight variation in the frequency at which optimal radiation occurs has been detected. This variation underscores the significance of the material properties, environmental factors, and the specific device employed. Nevertheless, the results indicate a commendable return loss across the studied frequency range of 3-12 GHz (Figure 26).

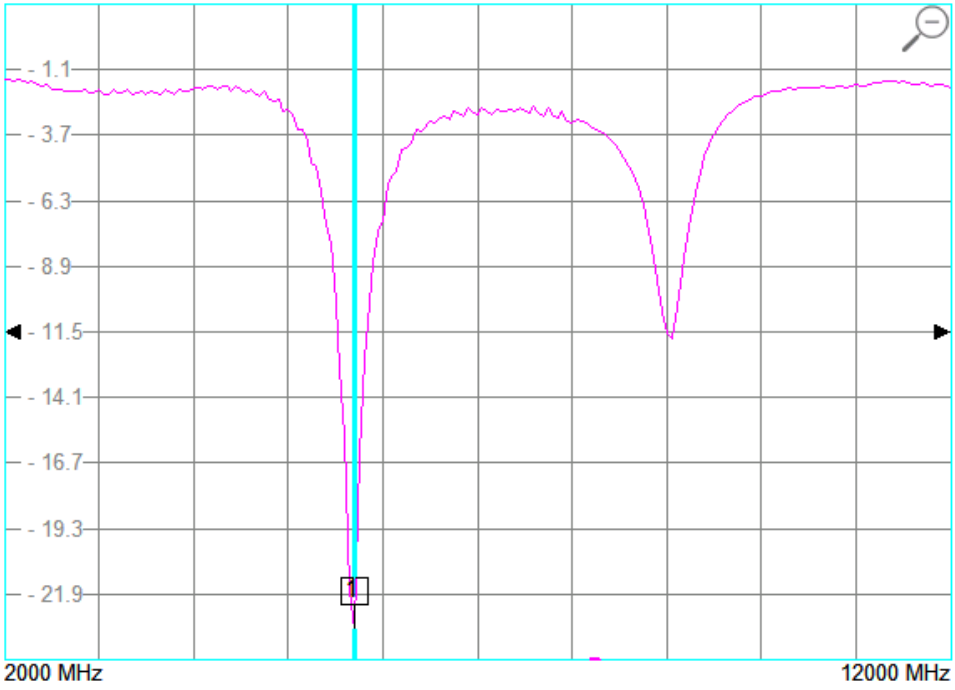

Figure 26. The FR-4 based antenna exhibits an S_{11} of -23.28 dB at 5.7 GHz.

The S_{11} return loss of the graphene-coated FR-4 plate is illustrated in Figure 27. The graphene-coated FR-4 plate exhibits superior performance at higher frequencies. In the simulation program, graphene is not selectable as a material within the GHz band; it is exclusively available for antennas operating in the THz band. This limitation is inadequate for our requirements. Consequently, simulations for the rGO-coated FR-4 could not be conducted. Only real-time tests have been performed, with measurements from the pure form of the FR-4 plate as a benchmark for comparison. The rGO-coated FR-4 plate demonstrates a significantly improved value of -27.63 dB at 9.15 GHz. This indicates that incorporating graphene leads to a markedly enhanced S_{11} value in the higher frequency range under investigation.

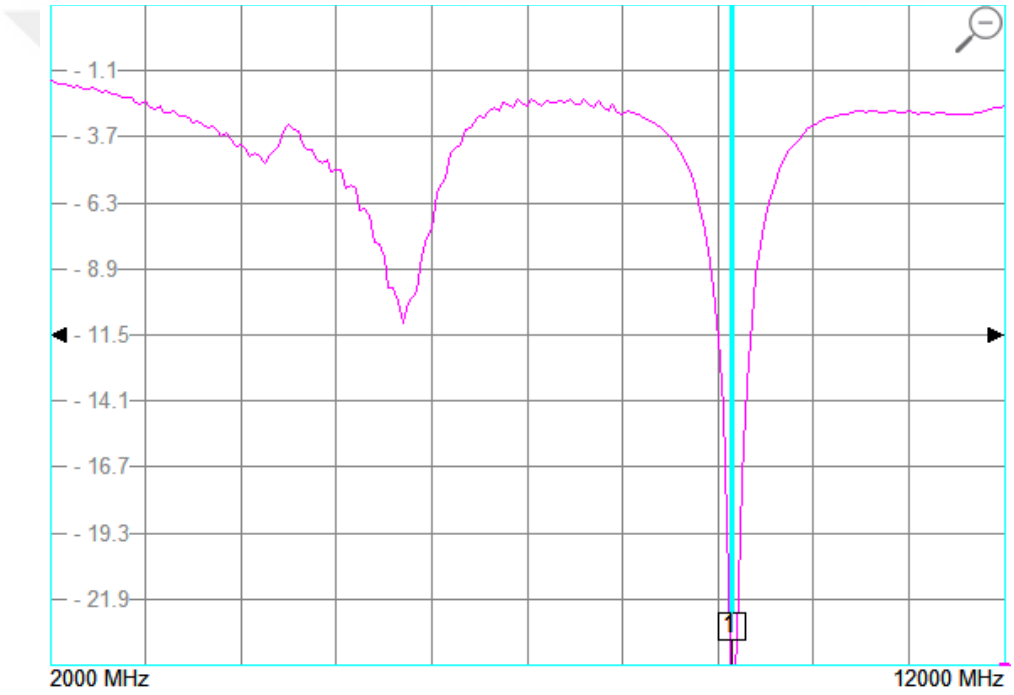

Figure 27. The FR-4 substrate coated with rGO exhibits an S_{11} of -27.63 dB at 9.15 GHz.

In the subsequent phase, evaluations were performed utilizing the Rogers RT-5880 board, which offers significantly enhanced features compared to the FR-4 board. The rationale for selecting the Rogers RT-5880 is outlined as follows:

- Maintains stable electrical characteristics across a broad frequency spectrum,
- Offers ease of cutting, shaping, and machining for precise fabrication,
- Exhibits strong resistance to chemical solvents and processing agents used in etching and plating procedures,
- Suitable for deployment in high-humidity or moisture-prone environments,

- Recognized as a reliable and industry-standard substrate material,
- Delivers exceptionally low dielectric losses among reinforced PTFE-based laminates.

The simulation was conducted using Rogers RT-5880 within the CST program. Similar to FR-4 boards, frequency discrepancies were noted. Nevertheless, the results obtained are consistent with the simulations performed. The Rogers RT-5880 board demonstrates superior performance at selected frequencies, with a loss of -22.99 dB recorded at 4.8 GHz, which is regarded as a commendable outcome within the studied frequency range (Figure 28).

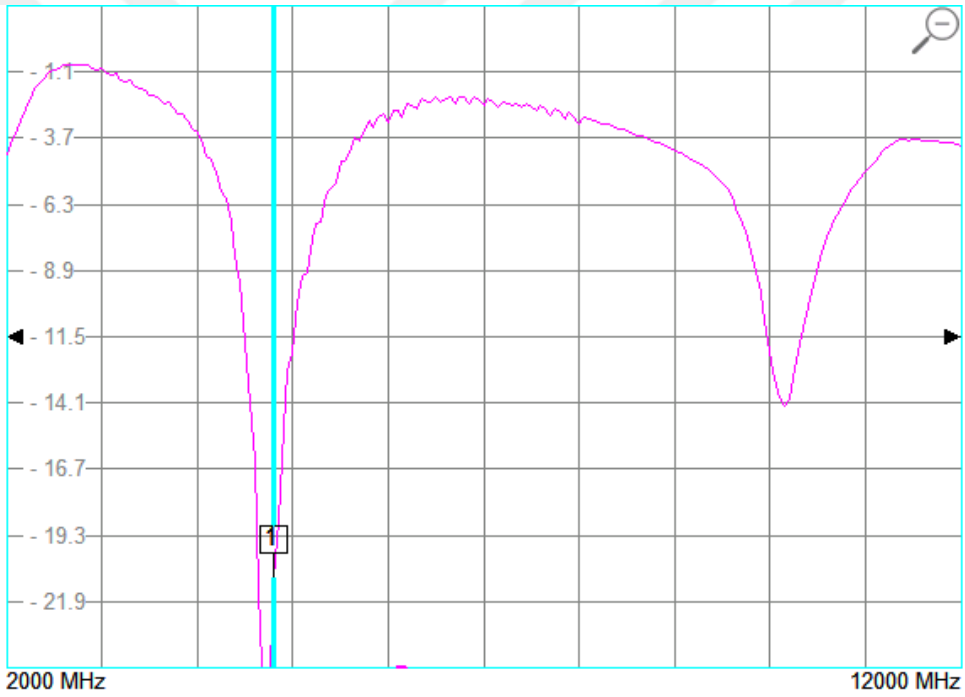

Figure 28. The antenna on the Rogers RT/duroid 5880 substrate shows an S_{11} of -22.99 dB at 4.8 GHz.

The real-time results of the graphene-coated Rogers RT-5880 board are presented in Figure 29. Comparisons are made based on measurement results rather than simulation outcomes for the Rogers RT-5880 board. Applying rGO coating on the boards enhances the S_{11} parameters and increases operating frequency value. This indicates that improved return losses are observed at elevated frequencies. The antenna constructed with the rGO-coated Rogers RT-5880 board achieves a return loss of -27.1 dB at 11.1 GHz.

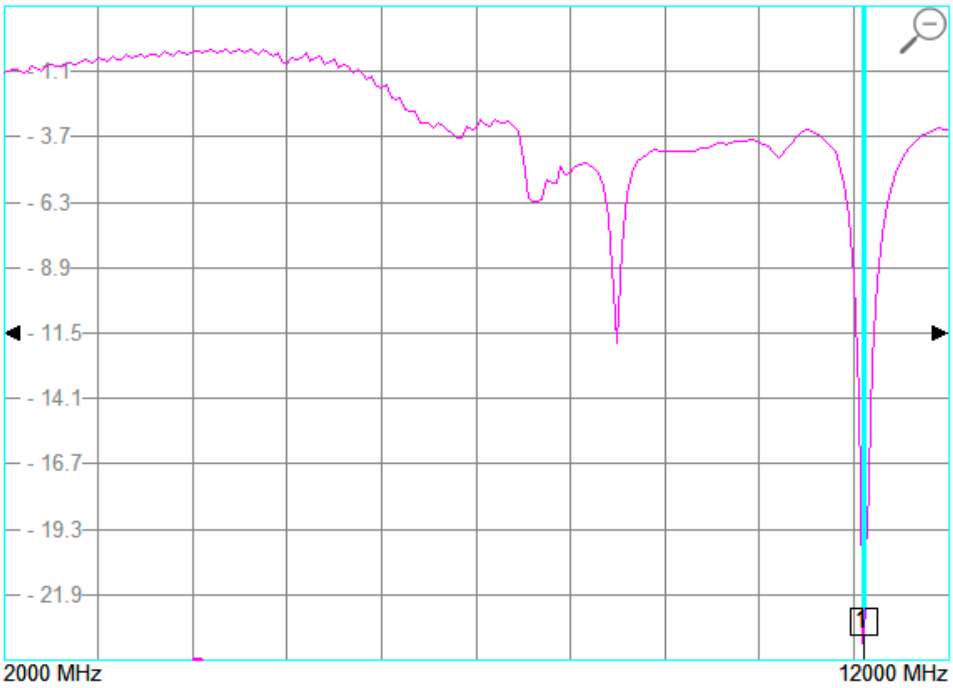

Figure 29. The antenna implemented on a rGO-coated Rogers RT/duroid 5880 substrate shows an S_{11} of -27.1 dB at 11.1 GHz.

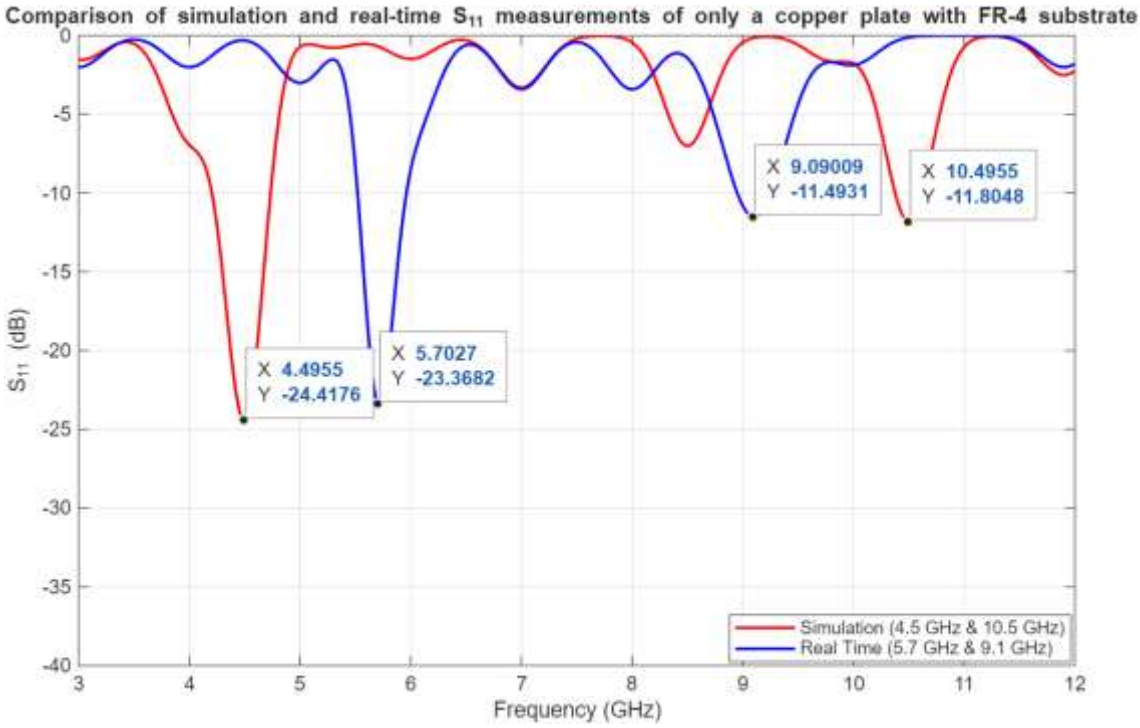

Figure 30. Comparison of simulation and real-time S_{11} measurements of only a copper plate with FR-4 substrate.

Figure 30 shows the comparison between simulation (red curve) and real-time measurement (blue curve) results for the return loss (S_{11}) of a copper-coated FR-4 substrate. The simulation curve exhibits two main resonant dips at approximately 4.5 GHz (−24.4 dB) and 10.5 GHz (−11.8 dB). These values indicate excellent impedance matching at the lower frequency and moderately good matching at the higher frequency within the simulated model.

In contrast, the real-time measurement results reveal resonances shifted slightly higher in frequency, with pronounced dips at around 5.7 GHz (−23.4 dB) and 9.1 GHz (−11.5 dB). The shift in resonant frequencies can be attributed to practical fabrication tolerances, variations in material properties, or differences between idealized simulation models and real-world conditions. Despite these shifts, the overall S_{11} magnitudes at the resonant points remain comparable between simulation and measurement, indicating that the design retains good impedance matching performance across both approaches. This comparison demonstrates that while simulation provides a reliable prediction of general trends and matching levels, slight frequency shifts should be expected in practical implementations.

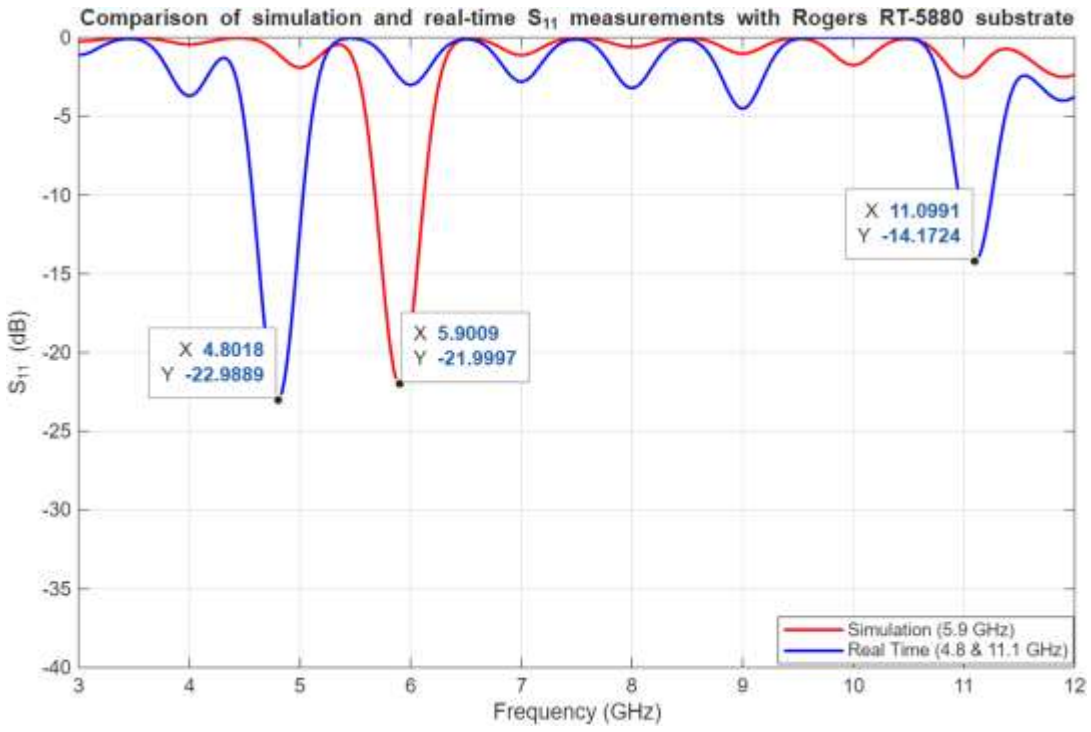

Figure 31. Comparison of simulation and real-time S_{11} measurements with Rogers RT-5880 substrate.

Figure 31 compares the return loss (S_{11}) results from simulation (red curve) and real-time measurement (blue curve) for the copper-coated Rogers RT-5880 substrate. The simulation shows a clear resonance at approximately 5.9 GHz with an S11 value of around −22 dB, indicating good impedance matching in the designed frequency band.

In the real-time measurements, two prominent resonances are observed at approximately 4.8 GHz (−23 dB) and 11.1 GHz (−14.2 dB). The first resonance appears at a lower frequency compared to the simulation, while an additional higher-frequency resonance emerges that is not predicted by the simulated model. These differences suggest that the real structure exhibits a broader operational bandwidth and more complex behavior, potentially due to fabrication tolerances, substrate anisotropy, or unmodeled parasitic effects in the physical prototype. Overall, while simulation provides an effective baseline prediction for the primary resonance, the measurements reveal extended bandwidth and highlight the importance of validating designs through experimental characterization.

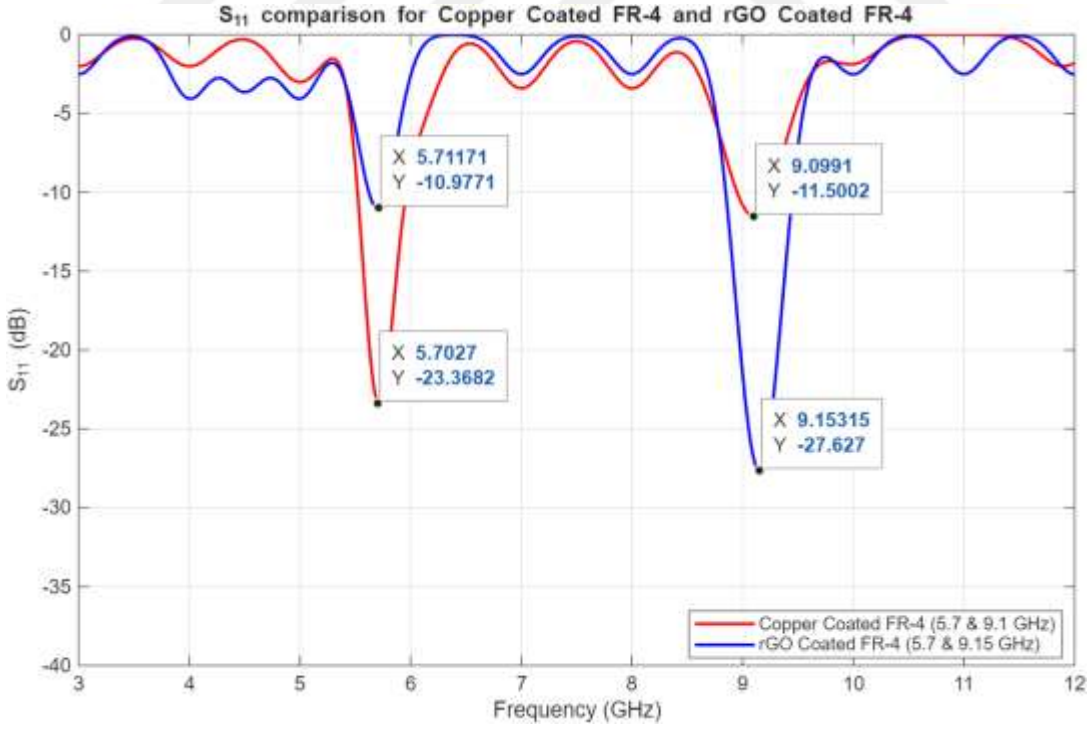

Figure 32. S_{11} comparison for Copper Coated FR-4 and rGO Coated FR-4.

Figure 32 compares the measured return loss (S_{11}) performance of FR-4 substrates coated with copper (red curve) and reduced graphene oxide (rGO, blue curve). Both coatings exhibit

resonances near 5.7 GHz and 9 GHz, but their return loss magnitudes differ significantly. At the lower-frequency resonance, the copper-coated FR-4 achieves approximately −23.4 dB at 5.7 GHz, while the rGO-coated FR-4 has a shallower dip near −11 dB at 5.71 GHz. However, at the higher-frequency resonance, rGO-coated FR-4 demonstrates a much deeper return loss of about −27.6 dB at 9.15 GHz compared to the copper-coated FR-4's −11.5 dB at 9.1 GHz.

These results indicate that while copper coating delivers better impedance matching at the lower resonance, rGO coating significantly improves return loss at higher frequencies, suggesting superior absorption or impedance-matching properties in that band. Additionally, the rGO-coated sample maintains similar bandwidth coverage (5.7–9.15 GHz) but achieves better overall S_{11} performance at critical points. This highlights the potential of rGO as an advanced coating material for enhancing high-frequency antenna performance and broadening operational bandwidth.

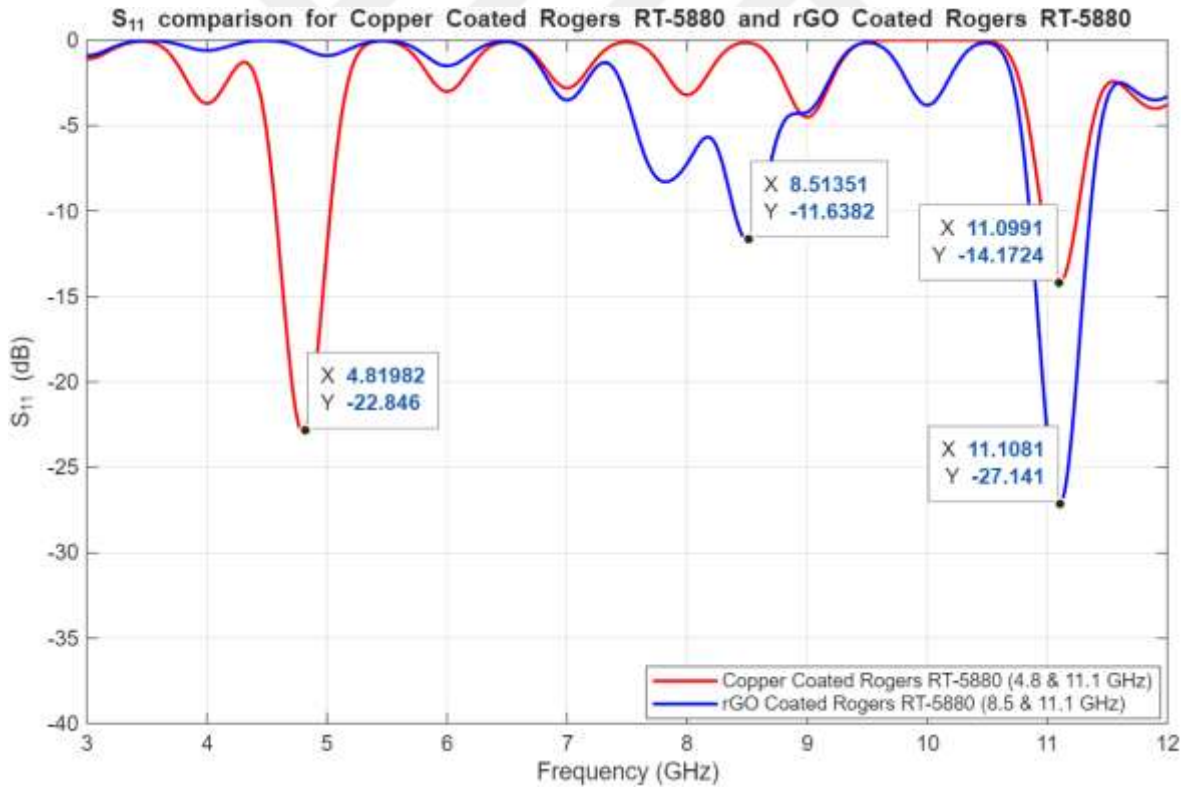

Figure 33. S_{11} comparison for Copper Coated Rogers RT-5880 and rGO Coated Rogers RT-5880.

Figure 33 compares the measured return loss (S_{11}) of Rogers RT-5880 substrates coated with copper (red curve) and reduced graphene oxide (rGO, blue curve). The copper-coated sample

shows a strong resonance at approximately 4.82 GHz with an S_{11} value of about −22.8 dB, and a higher-frequency dip around 11.1 GHz with an S_{11} of −14.2 dB. These results indicate effective impedance matching at both frequency points within the operational band.

In contrast, the rGO-coated Rogers RT-5880 exhibits broader and deeper resonances, with significant S_{11} dips at approximately 8.5 GHz (−11.6 dB) and 11.1 GHz (−27.1 dB). The rGO-coated sample clearly achieves much lower return loss at the higher-frequency resonance, indicating substantially improved matching and potential for reduced reflection. The overall bandwidth is also effectively extended, with the rGO layer enabling additional resonance features not present in the copper-coated counterpart. These findings suggest that rGO coatings can enhance high-frequency performance and broaden the operational range of Rogers RT-5880-based antenna structures, supporting their use in advanced broadband and high-frequency applications.

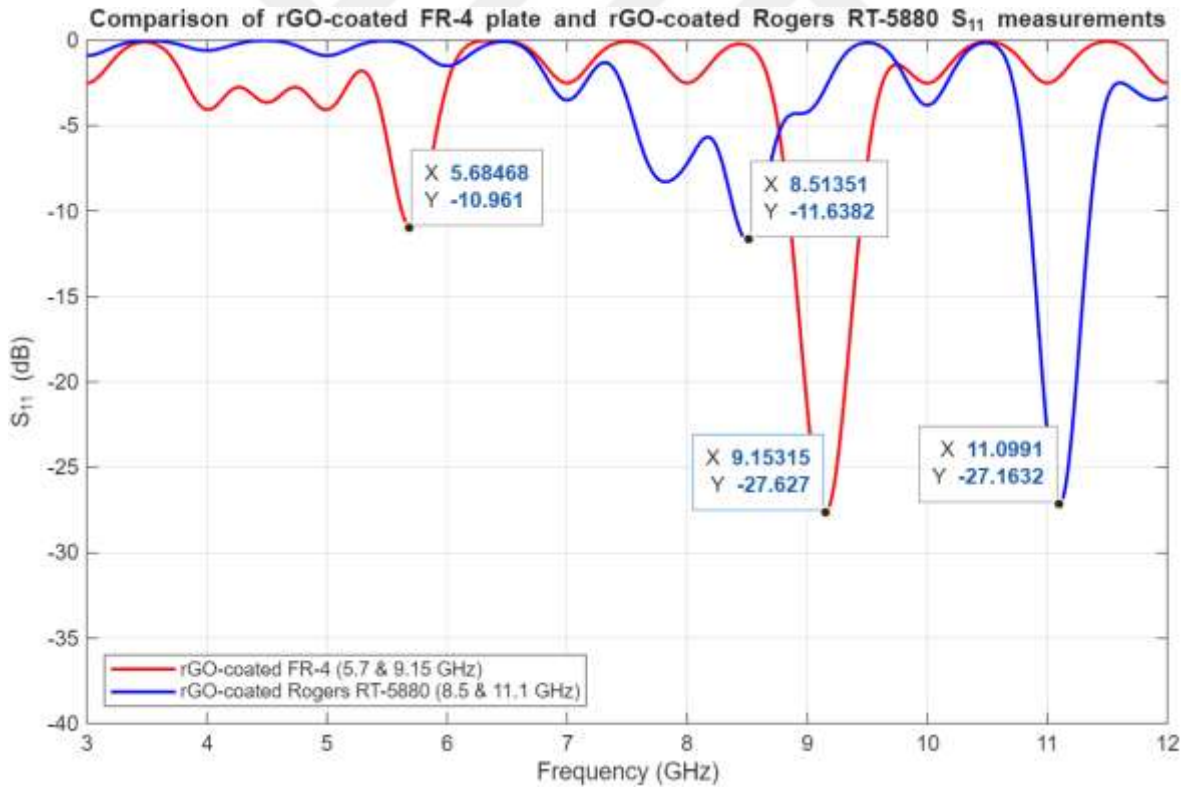

Figure 34. S_{11} comparison for rGO Coated FR-4 and rGO Coated Rogers RT-5880.

Figure 34 illustrates the measured return loss (S_{11}) characteristics of FR-4 and Rogers RT-5880 substrates, both coated with reduced graphene oxide (rGO). The rGO-coated FR-4 (red curve) exhibits primary resonances near 5.68 GHz (−11 dB) and 9.15 GHz (−27.6 dB),

showing moderate impedance matching at the lower frequency and excellent matching at the higher frequency.

In comparison, the rGO-coated Rogers RT-5880 substrate (blue curve) demonstrates broader and deeper resonances with key dips at approximately 8.51 GHz (−11.6 dB) and 11.1 GHz (−27.2 dB). These results highlight the superior high-frequency performance of the Rogers RT-5880 substrate when combined with rGO coating. Specifically, Rogers RT-5880 extends the operational bandwidth further into higher frequencies while maintaining comparable or better S_{11} values at resonance. Overall, this comparison underscores the benefit of using Rogers RT-5880 with rGO coatings for broadband, high-frequency antenna applications, offering improved impedance matching and wider usable frequency ranges compared to the FR-4 counterpart.

Table 3 shows the return loss (S_{11}) performance of different layer materials based on simulation results. The copper-coated FR-4 material achieves a very low S_{11} value of -24 dB at 4.5 GHz, indicating excellent impedance matching at that frequency, while this value increases to -11.8 dB at 10.5 GHz, suggesting a gradual degradation in matching with higher frequency. The copper-coated Rogers RT-5880 material demonstrates an S_{11} value of -22 dB at 5.9 GHz, also indicating good performance. Overall, the simulation results reveal that Rogers RT-5880 may maintain more stable characteristics at higher frequencies, and that both materials can achieve low return loss within certain frequency bands when coated with copper.

Table 3. Analysis of Alternative Layer Types and Return Loss with Frequency Values (Simulation Results)

Materials	**Minimum Frequency (GHz)**	**Maximum Frequency (GHz)**	**S_{11} (dB) value at minimum frequency**	**S_{11} (dB) value at maximum frequency**
Copper Coated FR-4	4.5 GHz	10.5 GHz	-24 dB	-11.8 dB
Copper Coated Rogers RT-5880	5.9 GHz	-	-22 dB	-

Table 4 presents real measurement results, offering a more detailed view of how coating types affect performance. The copper-coated FR-4 sample achieves S_{11} values ranging from -23.3 dB to -11.5 dB across the 5.7–9 GHz band, indicating good impedance matching. In comparison, rGO-coated FR-4 shows S_{11} values varying from -11 dB to -27.63 dB in nearly the same frequency range, with especially lower (better) return loss at higher frequencies. Similarly, the copper-coated Rogers RT-5880 performs across 4.8–10.1 GHz with S_{11} values between -22.99 dB and -14.1 dB, while rGO-coated Rogers RT-5880 achieves -11.6 dB to -27.1 dB over a broader 8.5–11.1 GHz range. These results demonstrate that rGO coating not only expands the operational bandwidth but also improves return loss at higher frequencies, making it an advantageous alternative for antenna design.

Table 4. Analysis of Alternative Layer Types and Return Loss with Frequency Values (Real-Time Results)

Materials	**Minimum Frequency (GHz)**	**Maximum Frequency (GHz)**	**S_{11} (dB) value at minimum frequency**	**S_{11} (dB) value at maximum frequency**
Copper Coated FR-4	5.7 GHz	9 GHz	-23.3 dB	-11.5 dB
rGO Coated FR-4	5.7 GHz	9.15 GHz	-11 dB	-27.63 dB
Copper Coated Rogers RT-5880	4.8 GHz	10.1 GHz	-22.99 dB	-14.1 dB
rGO Coated Rogers RT-5880	8.5 GHz	11.1 GHz	-11.6 dB	-27.1 dB

5. CONCLUSION AND RECOMMENDATIONS

Conclusion

This thesis presented the design, simulation, fabrication, and analysis of a novel graphene-based fractal microstrip patch antenna intended for wideband (WB) 5G applications. The antenna was designed to operate within the 3–12 GHz range and incorporated deterministic fractal structures to enhance miniaturization, multiband behavior, and radiation performance. Graphene, selected for its exceptional electrical, thermal, and mechanical properties, was successfully synthesized and applied to FR-4 and Rogers RT-5880 substrates via Electrophoretic Deposition (EPD).

Simulation studies using CST Studio Suite demonstrated excellent impedance matching and gain characteristics for conventional and graphene-coated structures. The measured S_{11} parameters, verified through Vector Network Analyzer (VNA) measurements, are closely aligned with simulation results, particularly regarding resonance frequency and return loss. Notably, the graphene-coated samples displayed enhanced performance at higher frequencies, with the graphene-coated Rogers RT-5880 board achieving an S_{11} of -27.1 dB at 10.1 GHz. This validates the effectiveness of graphene integration in expanding the operational bandwidth and improving reflection characteristics.

Introducing fractal geometries—implemented through hexagonal notching and 1/3 scaling techniques—yielded performance improvements consistent with those reported in the literature. Furthermore, experimental analysis using Raman spectroscopy and SEM verified the successful reduction of graphene oxide to rGO and its uniform deposition on antenna surfaces. This interdisciplinary integration of material science and microwave engineering has yielded a high-performance, low-profile antenna suitable for modern wireless systems.

Recommendations

While the thesis presents significant advancements, several aspects warrant further exploration and development:

a. Graphene can be integrated into an antenna using an advanced program. However, due to the limitations of the CST program in defining graphene materials within GHz bands, it is recommended to explore alternative software and models that facilitate graphene simulations in future applications.

b. Impedance Tuning Mechanisms: The application of reconfigurable components such as varactor diodes or MEMS switches can be investigated to enable dynamic resonance frequency and polarization tuning, particularly for adaptive 5G systems.

c. Environmental and Thermal Stability: Further studies should examine graphene-coated substrates' long-term behavior and environmental resilience under varying humidity and temperature conditions, especially for outdoor or wearable applications.

d. Alternative Substrate Materials: Although Rogers RT-5880 performed better than FR-4, other low-loss, flexible, or biocompatible substrates may be explored for specific use cases in biomedical or flexible electronics.

e. Array Configurations and MIMO Systems: Future research should focus on integrating the designed antenna into array structures, assessing its performance in multi-element systems such as MIMO, where inter-element coupling and beam steering capabilities are critical.

f. Advanced Coating Techniques: The uniformity and quality of graphene deposition via EPD can be further enhanced by optimizing parameters or exploring alternative deposition techniques such as spray-coating, chemical vapor deposition (CVD), or laser-induced methods.

The proposed antenna design can be advanced for commercial, military, and biomedical applications by addressing these areas, contributing to the broader adoption of graphene-based antenna technologies in next-generation wireless communication systems.

REFERENCES

Allen, M. J., Tung, V. C., & Kaner, R. B. (2010). Honeycomb Carbon: A Review of Graphene. *Chemical Reviews*, *110*(1), 132–145. https://doi.org/10.1021/cr900070d

Atiq Ur Rehman, M., Chen, Q., Braem, A., Shaffer, M. S. P., & Boccaccini, A. R. (2021). Electrophoretic deposition of carbon nanotubes: recent progress and remaining challenges. *International Materials Reviews*, *66*(8), 533–562. https://doi.org/10.1080/09506608.2020.1831299

Balanis, C. A. (2024). The Evolution of Antenna Technology: Reflectors and Microstrips. *IEEE Antennas and Propagation Magazine*, 2–10. https://doi.org/10.1109/MAP.2024.3457317

BESRA, L., & LIU, M. (2007). A review on fundamentals and applications of electrophoretic deposition (EPD). *Progress in Materials Science*, *52*(1), 1–61. https://doi.org/10.1016/j.pmatsci.2006.07.001

Bonaccorso, F., Sun, Z., Hasan, T., & Ferrari, A. C. (2010). Graphene photonics and optoelectronics. *Nature Photonics*, *4*(9), 611–622. https://doi.org/10.1038/nphoton.2010.186

Boutayeb, H., & Denidni, T. A. (2007). Gain Enhancement of a Microstrip Patch Antenna Using a Cylindrical Electromagnetic Crystal Substrate. *IEEE Transactions on Antennas and Propagation*, *55*(11), 3140–3145. https://doi.org/10.1109/TAP.2007.908818

Brida, D., Tomadin, A., Manzoni, C., Kim, Y. J., Lombardo, A., Milana, S., Nair, R. R., Novoselov, K. S., Ferrari, A. C., Cerullo, G., & Polini, M. (2013). Ultrafast collinear scattering and carrier multiplication in graphene. *Nature Communications*, *4*(1), 1987. https://doi.org/10.1038/ncomms2987

Choi, S. H., Park, J. K., Kim, S. K., & Park, J. Y. (2004). A new ultra-wideband antenna for UWB applications. *Microwave and Optical Technology Letters*, *40*(5), 399–401. https://doi.org/10.1002/mop.11392

Choi, W., Lahiri, I., Seelaboyina, R., & Kang, Y. S. (2010). Synthesis of Graphene and Its Applications: A Review. *Critical Reviews in Solid State and Materials Sciences*, *35*(1), 52–71. https://doi.org/10.1080/10408430903505036

Constantine A. Balanis. (2012). *ADVANCEDENGINEERING ELECTROMAGNETICS* (SECOND EDITION). John Wiley & Sons, Inc.

Constantine A. Balanis. (2016). *ANTENNA THEORY ANALYSIS AND DESIGN* (THIRD EDITION). A JOHN WILEY & SONS, INC., PUBLICATION.

Dappe, Y. J., Basanta, M. A., Flores, F., & Ortega, J. (2006). Weak chemical interaction and van der Waals forces between graphene layers: A combined density functional and intermolecular perturbation theory approach. *Physical Review B*, *74*(20), 205434. https://doi.org/10.1103/PhysRevB.74.205434

de Sousa, F. M., de Sousa, F. B., Miranda, I. R. S., de Oliveira, J. E., Paschoal, W., & Costa, M. B. C. (2023). Graphene based nano patch antenna using photonic band gap insertion into substrate for applications at THz band. *Optical and Quantum Electronics*, *55*(3), 210. https://doi.org/10.1007/s11082-022-04394-0

Demirkoparan, B. N., & Basdemir, H. D. (2024). Graphene Based Fractal Structure 5G Microstrip Patch Antenna Design. *2024 15th National Conference on Electrical and Electronics Engineering (ELECO)*, 1–5. https://doi.org/10.1109/ELECO64362.2024.10847214

Dobir Hossain, S., Sobahan, K. M. A., Hossain, Md. K., Ahamed Akash, Md. M., Sultana, R., & Billah, Md. M. (2016). A Rectangular Microstrip Patch Antenna for Wireless Communications Operates in Dual Band. *International Journal of Wireless and Microwave Technologies*, *6*(5), 35–44. https://doi.org/10.5815/ijwmt.2016.05.04

Esin Chang, Long, S., & Richards, W. (1986). An experimental investigation of electrically thick rectangular microstrip antennas. *IEEE Transactions on Antennas and Propagation*, *34*(6), 767–772. https://doi.org/10.1109/TAP.1986.1143890

Falkovsky, L. A. (2008). Optical properties of graphene and IV–VI semiconductors. *Physics-Uspekhi*, *51*(9), 887–897. https://doi.org/10.1070/PU2008v051n09ABEH006625

Gourav Misra, A. A. K. A. (2015). Design and Performance Evaluation of Microstrip Antenna for Ultra-Wideband Applications Using Microstrip Feed. *American Journal of Electrical and Electronic Engineering*, *3*, 93–99.

Hafez, H. A., Kovalev, S., Deinert, J.-C., Mics, Z., Green, B., Awari, N., Chen, M., Germanskiy, S., Lehnert, U., Teichert, J., Wang, Z., Tielrooij, K.-J., Liu, Z., Chen, Z., Narita, A., Müllen, K., Bonn, M., Gensch, M., & Turchinovich, D. (2018). Extremely

efficient terahertz high-harmonic generation in graphene by hot Dirac fermions. *Nature*, *561*(7724), 507–511. https://doi.org/10.1038/s41586-018-0508-1

Hossain, D., Hossain, M. K., & Sultana, R. (2016). I C 4 M E 2 Proceedings Design of a Linearly Polarized Multi-band Transmission Line Feed Microstrip Patch Antenna for Wireless Communications. In *Materials and Electronic Engineering IC* (Vol. 4).

Jamil, M. F., Biçer, E., Yarar Kaplan, B., & Alkan Gürsel, S. (2021). One-step fabrication of new generation graphene-based electrodes for polymer electrolyte membrane fuel cells by a novel electrophoretic deposition. *International Journal of Hydrogen Energy*, *46*(7), 5653–5663. https://doi.org/10.1016/j.ijhydene.2020.11.039

John Coonrod. (2023). Material Factors Affect Microstrip Patch Antennas. *Microwave Journal*.

Jung, D., Park, C. J., Kwon, T. S., Seo, J. W., Ahn, B., Wi, S. H., & Na, I. (2024). Terahertz Antenna-in-Package Design and Measurement for 6G Communications Systems. *IEEE Transactions on Antennas and Propagation*, *72*(2), 1085–1096. https://doi.org/10.1109/TAP.2023.3320276

Karmakar, A. (2021). Fractal antennas and arrays: a review and recent developments. *International Journal of Microwave and Wireless Technologies*, *13*(2), 173–197. https://doi.org/10.1017/S1759078720000963

Kazama, Y. (n.d.). *A Novel Wideband Circular PolaIization Microstrip Antenna-Combination ofdifferent shaped antenna element-Takanon NORO* ad*.

Kumar, C., Raghuwanshi, S. K., & Kumar, V. (2022). Graphene based microstrip patch antenna on photonic crystal substrate for 5G application. *Frontiers in Materials*, *9*. https://doi.org/10.3389/fmats.2022.1079588

Liu, H., Liu, Y., & Zhu, D. (2011). Chemical doping of graphene. *J. Mater. Chem.*, *21*(10), 3335–3345. https://doi.org/10.1039/C0JM02922J

M. A. Peyrot-Solis, G.M. Galvan-Tejada, & H. Jardon-Aguilar. (2005). *2005 2nd International Conference on Electrical and Electronics Engineering (ICEEE) : Mexico City, Mexico, September 7-9, 2005*. IEEE.

Marhoon, H. M., & Qasem, N. (2020). Simulation and optimization of tuneable microstrip patch antenna for fifth-generation applications based on graphene. *International*

Journal of Electrical and Computer Engineering (IJECE), *10*(5), 5546. https://doi.org/10.11591/ijece.v10i5.pp5546-5558

Mishra, B., Singh, A. K., Satheesha, T. Y., Verma, R. K., & Singh, V. (2024). From Past to Present: A Comprehensive Review of Antenna Technology in Modern Wireless Communication. In *Journal of Engineering Science and Technology Review* (Vol. 17, Issue 3, pp. 179–200). International Hellenic University School of Science and Technology. https://doi.org/10.25103/jestr.173.20

Mohammad Khani, A. A., Fouladian, M., & Mazloum, J. (2023). Multi layers THz duplexer based on combined graphene patterns. *Solid State Communications*, *360*, 114974. https://doi.org/10.1016/j.ssc.2022.114974

Nagy, L. (2023). Microstrip Antenna Development for Radar Sensor. *Sensors*, *23*(2). https://doi.org/10.3390/s23020909

Niu, K., Li, P., Huang, Z., Jiang, L. J., & Bagci, H. (2020). Numerical Methods for Electromagnetic Modeling of Graphene: A Review. *IEEE Journal on Multiscale and Multiphysics Computational Techniques*, *5*, 44–58. https://doi.org/10.1109/JMMCT.2020.2983336

Pang, Y. H., & Wu, R. B. (2002). Analysis of microstrip antennas with inhomogeneous and finite-sized substrate. *IEEE Antennas and Propagation Society, AP-S International Symposium (Digest)*, *1*, 789–792. https://doi.org/10.1109/aps.2002.1016461

Paun, M., Nichita, M., Paun, V., & Paun, V. (2025). Fifth-generation fractal antenna design based on the <scp>Koch S</scp> nowflake geometry. A fractal theory application. *Expert Systems*, *42*(1). https://doi.org/10.1111/exsy.13242

Pop, E., Varshney, V., & Roy, A. K. (2012). Thermal properties of graphene: Fundamentals and applications. *MRS Bulletin*, *37*(12), 1273–1281. https://doi.org/10.1557/mrs.2012.203

Qamar, T., Halder, N., Siddiqui, M. G., & Varshney, V. (n.d.). *SIMULATION AND ANALYSIS OF SLOT-COUPLED PATCH ANTENNA AT DIFFERENT FREQUENCIES USING HFSS* (Vol. 3, Issue 3). www.jifactor.com

Rochman, M. I., Ye, W., Zhang, Z.-L., & Ghosh, M. (2025). A Comprehensive Real-World Evaluation of 5G Improvements over 4G in Low-and Mid-Bands. *IEEE Transactions*

on Cognitive Communications and Networking, 1–1. https://doi.org/10.1109/TCCN.2025.3558062

Süzgün, M., & Cansiz, M. (2024). Design and implementation of multiband microstrip antenna for energy harvesting. *DÜMF Mühendislik Dergisi*. https://doi.org/10.24012/dumf.1440939

Targonski, S. D., Waterhouse, R. B., & Pozar, D. M. (1998). Design of Wide-Band Aperture-Stacked Patch Microstrip Antennas. In *IEEE TRANSACTIONS ON ANTENNAS AND PROPAGATION* (Vol. 46, Issue 9).

Tielrooij, K. J., Piatkowski, L., Massicotte, M., Woessner, A., Ma, Q., Lee, Y., Myhro, K. S., Lau, C. N., Jarillo-Herrero, P., van Hulst, N. F., & Koppens, F. H. L. (2015). Generation of photovoltage in graphene on a femtosecond timescale through efficient carrier heating. *Nature Nanotechnology*, *10*(5), 437–443. https://doi.org/10.1038/nnano.2015.54

Venkatrao*, K., Priya, S. H., Raghavendra, R., Kiran, M. N. S., & Sumanth, D. (2020). Multi Band Minswoki Fractal Antenna for 5G Applications. *International Journal of Recent Technology and Engineering (IJRTE)*, *8*(6), 3525–3530. https://doi.org/10.35940/ijrte.F8605.038620

Viti, L., & Vitiello, M. S. (2021). Tailored nano-electronics and photonics with two-dimensional materials at terahertz frequencies. *Journal of Applied Physics*, *130*(17). https://doi.org/10.1063/5.0065595

Warren L. Stutzman, G. A. T. (2012). *Antenna Theory and Design* (THIRD EDITION). John Wiley & Sons.

Younssi, M., Jaoujal, A., El Moussaoui, A., & Aknin, N. (n.d.). *Miniaturized Probe-Fed Elliptical Microstrip Patch Antenna for Radiolocation Applications*.

Zhang, H., Krooswyk, S., & Ou, J. (2015). Measurement and data acquisition techniques. In *High Speed Digital Design* (pp. 199–219). Elsevier. https://doi.org/10.1016/B978-0-12-418663-7.00005-8

Zhu, Y., Murali, S., Cai, W., Li, X., Suk, J. W., Potts, J. R., & Ruoff, R. S. (2010). Graphene and Graphene Oxide: Synthesis, Properties, and Applications. *Advanced Materials*, *22*(35), 3906–3924. https://doi.org/10.1002/adma.201001068

CURRICULUM VITAE

Personal Information

Name Surname

Date of Birth

E-mail

Education

Degree	Education Unit	Year
M. Sc.	SBTÜ/ Electrical-Electronics Engineering	2022
B. Sc.	SCÜ / Electrical-Electronics Engineering	2021

Academic Titles

Year	University	Degree
2024	Sivas University of Science and Technology	Research Assistant

Foreign Language

English

YOKDIL: 82.5

Publications

Book Chapters

- Husnu Deniz BASDEMIR, Beyza Nur DEMIRKOPARAN (2023). Diffraction Methods Approach to the Noise Shielding of Air Vehicles. Current Topics in Aeronautics (page 17). https://dx.doi.org/10.5281/zenodo.10390372
- Husnu Deniz BASDEMIR, Beyza Nur DEMIRKOPARAN (2025). Smart Antenna Systems and Applications: A Review. Aviation Technologies and Applications E-ISBN:978-605-338-471-7 2025, chap. (4), pp.59-74.

Papers presented at scientific meetings and published in the proceedings book

- Beyza Nur DEMIRKOPARAN, Husnu Deniz BASDEMIR (2025). Performance Analysis of a Graphene-Coated Fractal Microstrip Patch Antenna for 5G

Applications. 5th International Artificial Intelligence and Data Science Congress (ICADA 2025) E-ISBN: 978-625-95496-4-4.

Publications published in IEEE

- Beyza Nur DEMIRKOPARAN, Husnu Deniz BASDEMIR (2024). Graphene Based Fractal Structure 5G Microstrip Patch Antenna Design. 15th National Conference on Electrical and Electronics Engineering (ELECO). IEEE. https://doi.org/10.1109/ELECO64362.2024.10847214.

Projects

Graphene Based Fractal Structure 5G Microstrip Patch Antenna and Metamaterial Design with Production, BAP, 2023-GENL-Hav-0013 (Student).

SİVAS
BİLİM VE TEKNOLOJİ
ÜNİVERSİTESİ

KÖKLERDEN GÖKLERE…